BULLETIN OF THE EARTHQUAKE
RESEARCH INSTITUTE
Vol. 53 (1978), pp. 1-48

1. *Spectral Analysis of the Coda Waves from Local Earthquakes.*

By Masaru TSUJIURA,
Earthquake Research Institute.

(Received Jan. 31, 1978)

Abstract

Spectral content and decay characteristics with time of the coda waves from local earthquakes are studied using the data of narrow band-pass filters of six stations distributed in the Kanto district, Japan, and some properties of the effects of attenuation, excitation and radiation at the source on the coda waves are obtained. The decay characteristics of coda waves determined at a given station are independent of the epicenter location and source size, and depend only upon the duration time measured from the origin time as suggested by AKI (1969). The apparent Q derived from the coda waves at four stations increase with frequency, approximately proportionally to the square root of the frequency, with the values increasing from 120-250 at 0.75 Hz to 800-2500 at 24 Hz. The coda excitation at the six stations located on different geological formations also depends on frequency. The difference of coda amplitudes measured at the same lapse time between the stations located on the sediment and the granitic rocks is, on the average 20 times at 0.75 Hz and less than 1/10 at 24 Hz. This behavior suggests the differences in intrinsic Q and inhomogeneity size of the earth's crust beneath the station. The scaling laws of the earthquake source spectra are constructed using the spectral ratios of coda source factors and the source spectrum of the smallest earthquake used in the estimation of coda source factors. The local variation of the source spectrum is found within the area of the Kanto district, which may be attributed to the difference in rupture strength of the earth's crust.

1. Introduction

The investigation on the seismic source spectra of local earthquakes is important for elucidating regional tectonic features. Regional and local variations of seismic moments, source dimensions and stress drops of earthquakes in the California and Nevada regions are suggested by several authors, and are discussed in terms of the tectonic features of their regions (WYSS and BRUNE, 1971; DOUGLAS and RYALL, 1972; THATCHER, 1972; THATCHER and HANKS, 1973). However, the data on direct waves

such as *P*- and *S*-waves of local earthquakes must be carefully used for this purpose since high frequency seismic waves in the range up to 100 Hz contained in their seismograms are extremely sensitive to the details of the wave path and the geologic formation of the station site. For example, there are large local variations of *S*-wave spectra of small earthquakes in the Kanto district, Japan, and at least two times the difference of the quality factor Q seems to exist even for a given station (TSUJIURA, 1973a).

OMOTE (1943) studied the nature of coda waves from near and regional earthquakes observed at arrival time, at least five minutes, after *P*-wave arrivals. He pointed out that there exists a predominant period, and this period is nearly independent for the differences of epicentral distance (100–400 km), location and geology of the station site.

Recently AKI (1969) suggested that the seismic coda waves of local earthquakes are backscattering waves from numerous randomly distributed heterogeneities in the earth, and power spectra of coda waves decay only as a function of time measured from earthquake origin time, independent of the distance and the nature of the wave path. Based on the above assumption, he devised a method to extract useful information about the earthquake source from coda waves. The use of random media in seismogram interpretation has been attemted by several authors including TAKANO (1971), CLEARY and HADDAN (1972), AKI (1973) and CAPON (1974). AKI and CHOUET (1975) and CHOUET (1976) clearly demonstrated that Aki's assumption is supported for the coda waves of local earthquakes in several areas, and obtained important information about source, attenuation and scattering effects on coda waves.

The spectral content of earthquake motion changes systematically with the earthquake magnitude in a given seismic area. The manner in which the spectrum changes with magnitude is called the scaling law of the seismic spectrum (AKI, 1967). A theoretical scaling law of far-field seismic spectra based on the ω-square model has been proposed by AKI (1967). Later, he proposed the revised model B in order to explain the observations for earthquakes with $Ms<6$ and for period $T<10$ sec (AKI, 1972). However, the scaling law may be different for different seismic regions (TSUJIURA, 1973b). A reliable scaling law using the data of smaller earthquakes would give us a basis for predicting strong motion of a large earthquake in the same seismic area. Since the number of earthquakes increases exponentially with the decreasing magnitude, the data collection of small earthquakes is much more efficiently done. There appears to be a correlation between the source spectrum of small and large earthquakes in each area. The locus of corner frequency of small earthquakes will be extrapolated to large earthquakes in the same area (in preparation).

The subject of this paper is to investigate the effects of source properties, attenuation and scattering on coda waves of local earthquakes in the Kanto district by using a spectral analyzing seismograph. Three sets of identical analyzers are prepared in order to obtain the coda spectra at many stations and to compare observed coda waves of the same earthquake at different stations.

Furthermore, the study of the effect of superficial geological formations on coda waves as well as body waves is another subject, because it may be useful for seismic zoning in the field of earthquake engineering.

The scaling law of source spectra can be obtained from the ratios of source factors of coda waves and the source spectra of the smallest earthquakes corrected for local Q (AKI and CHOUET, 1975). Using their method, the scaling law of source spectra for the earthquakes in the Kanto district will be obtained over a wide frequency band. We shall show that a significant difference in the scaling laws for source spectra exists within the Kanto district, which will be attributed to variations in strength of the earth's crust.

It should be emphasized that the spectral study of coda and body waves for a wide frequency band on a basis of routine observation provides a promising method in finding temporal variations in source conditions and in attenuation properties as suggested by FEDOTOV *et al.* (1972), CHOUET (1976) and TSUJIURA (1977).

2. Spectrum analyzer

In order to obtain a large amount of running spectra of coda waves as a routine observation, an analogue type spectrum analyzer is used. A detailed description of the analyzer system was given by TSUJIURA (1966, 1967, 1969). A brief outline of the system will be described in the following.

The analyzer consists of one amplifier, six band-pass filters with center frequencies at 0.75, 1.5, 3, 6, 12 and 24 Hz, and respective bandwidths of 0.5, 1, 2, 4, 8 and 16 Hz. In addition, high frequency bands centered at 48 and 96 Hz with respective bandwidths of 32 and 64 Hz are used in some cases. The output of the six or eight filters is recorded continuously on an ink-writing 6-channel or 8-channel recorder. The input of the amplifier is connected to the output of the seismic telemetering network in the Kanto district. Three sets of the identical analyzers are used in order to compare the coda spectra of the same earthquake at different stations.

The location of the stations with their local geology are given in Fig. 2.1 and Table 1. The displacement magnification curve of the seismo-

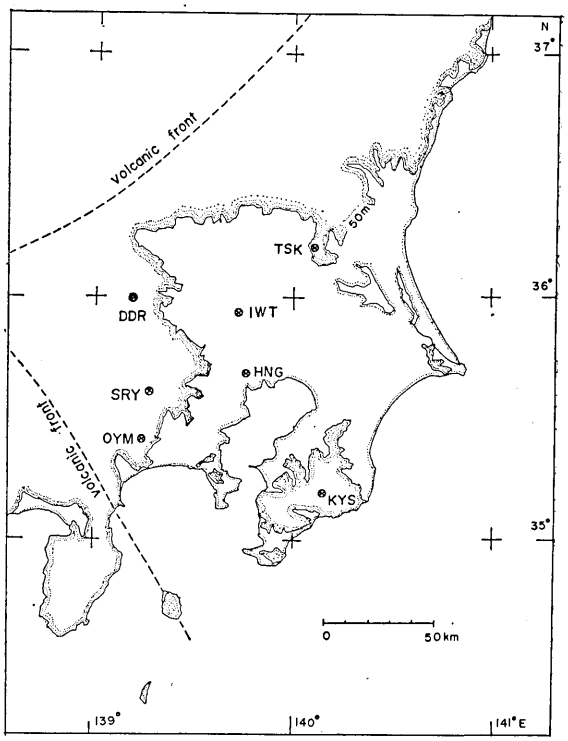

Fig. 2.1. Distribution of seismograph stations used in the coda wave analysis. All seismic signals are telemetered by radio waves to Earthquake Research Institute (HNG). IWT belongs to the National Research Center for Disaster Prevention.

Table 1. List of seismic stations used in the coda wave analysis. *: belong to the National Research Center for Disaster Prevention.

Station	Code	Location	Altitude	Formation
Tsukuba	TSK	36°12′39″0 N 140 06 35.0 E	280 m	Granite
Dodaira	DDR	35 59 54.0 N 139 11 36.2 E	800 m	Crystalline schist
Kiyosumi	KYS	35 11 51.6 N 140 08 53.6 E	180 m	Sandstone (Tertiary shale)
Ohyama	OYM	35 25 12.3 N 139 14 34.9 E	600 m	Andesite
Hongo	HNG	35 42 56 N 139 45 47 E	19 m	Loam
Iwatsuki*	IWT	35 55 33 N 139 44 17 E	−3502 m	Quartz porphyry

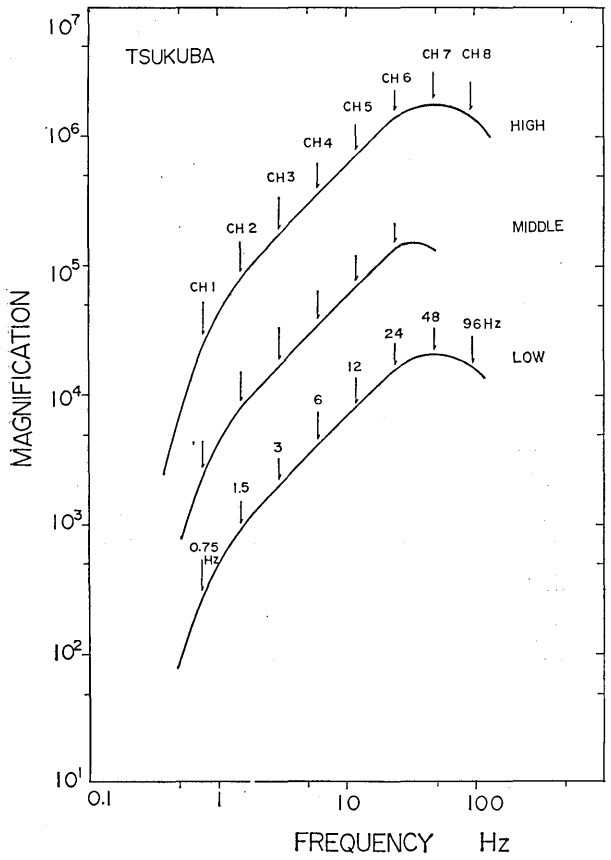

Fig. 2.2. Magnification curves of the seismographs for the Tsukuba station (TSK). Arrows show the channel number of the band-pass filter and its center frequency, respectively.

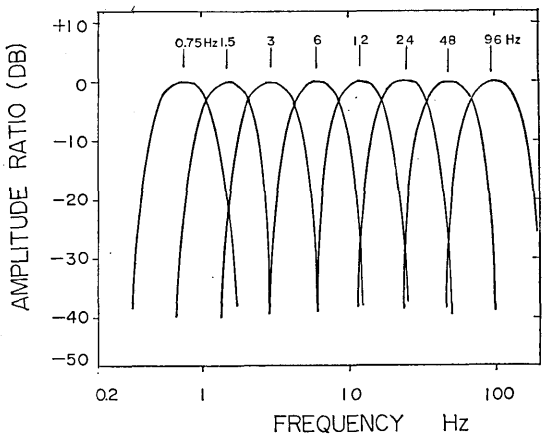

Fig. 2.3. Frequency response curves of band-pass filters used in the coda and S waves analysis. The frequencies from 0.75 to 96Hz indicate the center frequency (f_0) for each band-pass filter.

graphs at the Tsukuba station (TSK), and the filter response which has the same frequency characteristics for the three sets are shown in Figs. 2.2 and 2.3. All seismic signals are taken from a horizontal E-W component seismograph at each station. The frequency characteristics at most of the station used here are the same as that of TSK marked as "middle" in Fig. 2.2, although the magnification is somewhat different from station to station.

3. Data and method of analysis

Observational data are analyzed for the events with epicentral distance mainly less than 100 km from each station, and focal depth ranging from 40 to 160 km, which is classified into two depth ranges of 40–80 km and 100–160 km. The magnitudes of these events are between 1.5 and 5.8. The epicenter information of these events is taken from the monthly lists currently determined at the Earthquake Research Institute. As a basic set of data for the present analysis, observational records of about 350 earthquakes are available during the period of 1974–1976.

An example of the band-pass filter records obtained at Tsukuba station (TSK) is shown in Fig. 3.1, for two earthquakes with magnitudes 4.7 and 3.4. Similar filter-records are obtained at Dodaira (DDR), Ohyama

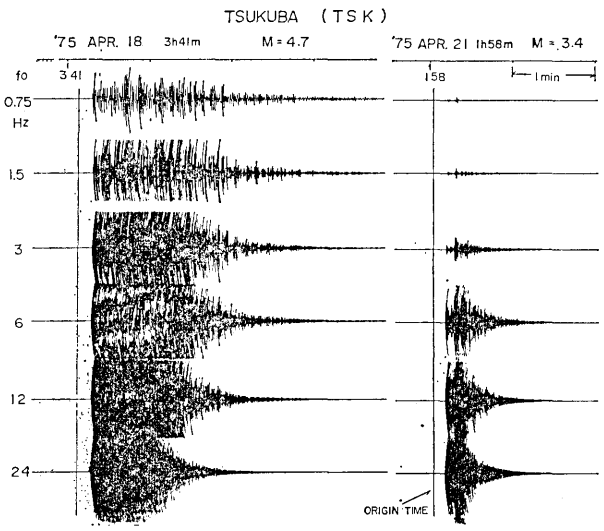

Fig. 3.1. An example of the filtered seismograms of two events with magnitudes 4.7 (left) and 3.4 (right) obtained at TSK. Center frequencies of band-pass filters are indicated on the left side of the figure. Tick marks at the top are minute marks. Magnitude M are determined by the total duration method.

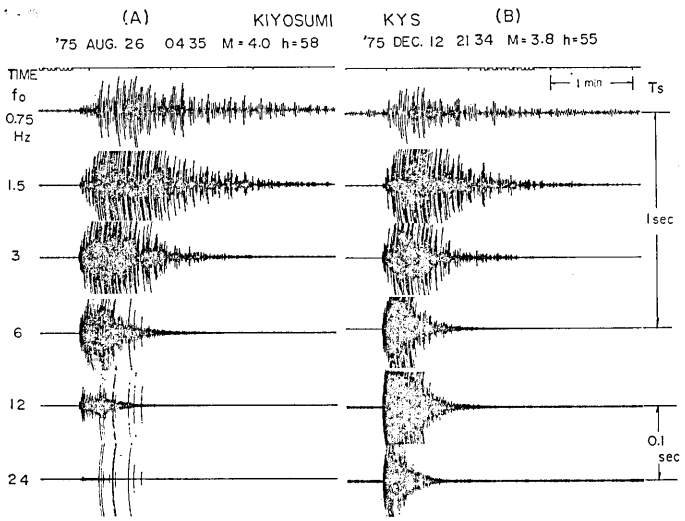

Fig. 3.2. An example of the filtered seismograms of two events obtained by different seismographs at KYS. Left side seismograms and upper four seismograms on the right side are obtained by a seismometer with a natural period of 1 sec and a damping constant of 0.5. Lower two seismograms on the right side are obtained by a seismometer with a natural period of 0.1 sec and a damping constant of 2. Explanation of the other symbols is the same for those of Fig. 3.1.

(OYM), Kiyosumi (KYS), Iwatsuki (IWT) and Hongo (HNG).

Fig. 3.2 shows an example of the records at KYS. As is shown for the event A, high frequency coda waves are more attenuated at KYS than TSK, and the coda waves of the 24 Hz band cannot be detected. Large impulsive amplitudes on the 12 Hz and 24 Hz bands are harmonics caused by the saturation of the amplifier. Therefore, as is shown for the event B, the records of the 12 and 24 Hz bands are taken from the output of the high frequency seismometer with a natural period of 0.1 sec

Table 2. The displacement magnification of seismographs used in Kiyosumi (KYS).

CH	f_0 Hz	Magnification	
		1 sec	0.1 sec
1	0.75	12.5×10^3	7.5×10^2
2	1.5	38.0×10^3	4.5×10^3
3	3.0	67.0×10^3	26.0×10^3
4	6.0	13.0×10^4	13.0×10^4
5	12.0	25.0×10^4	58.0×10^4
6	24.0	40.0×10^4	16.0×10^5

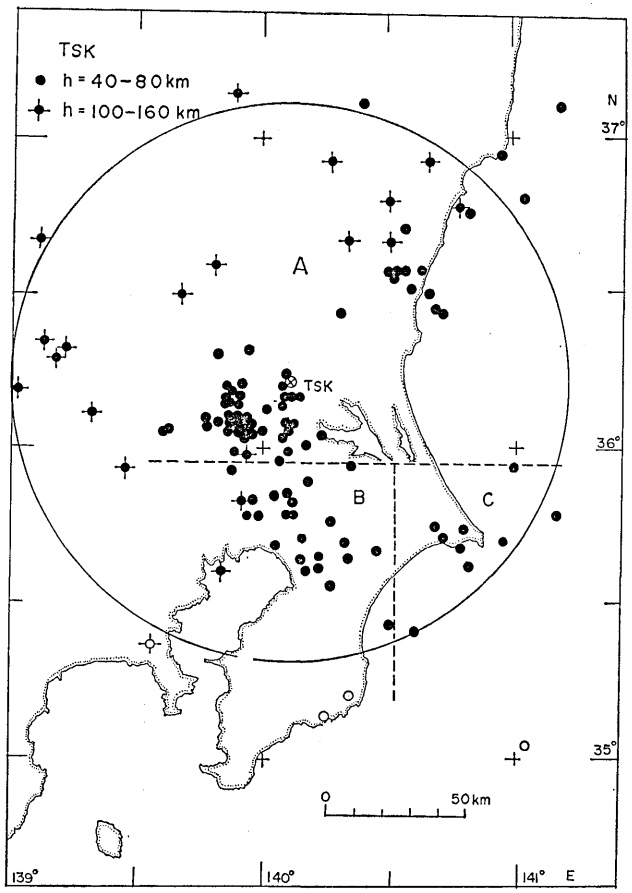

Fig. 3.3a. Epicenter locations of earthquakes used in the coda wave analysis at TSK. Closed circles indicate events with source depths (h) between 40 and 80 km, and closed circles with cross mark are those of 100 and 160 km. Dashed lines represent the boundary of the areas.

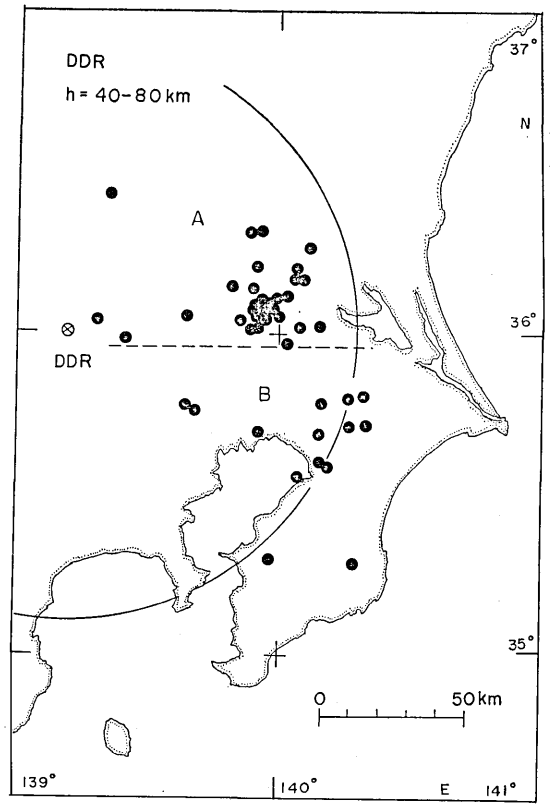

Fig. 3.3b. Epicenter locations of earthquakes used in the coda analysis at DDR. Explanation of the symbols is the same for those of Fig. 3.3a.

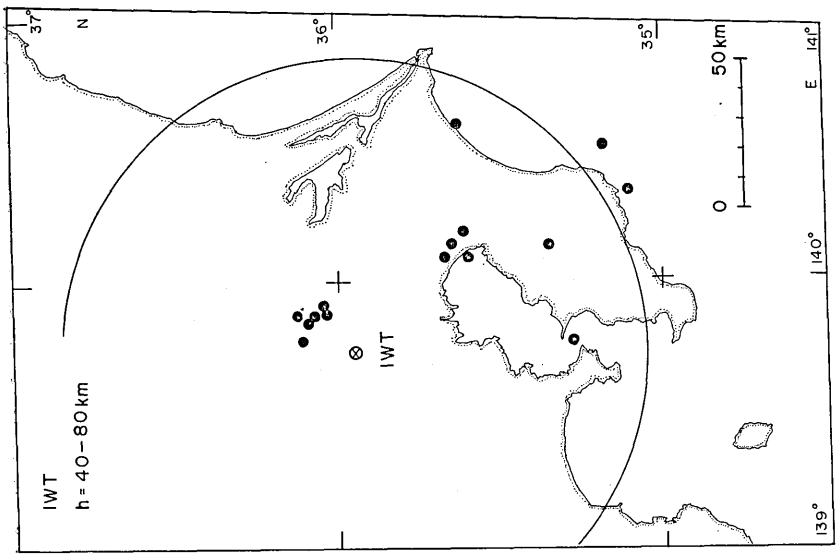

Fig. 3.3d. Epicenter locations of earthquakes used in the coda analysis at IWT. Explanation of the symbols is the same for those of Fig. 3.3a.

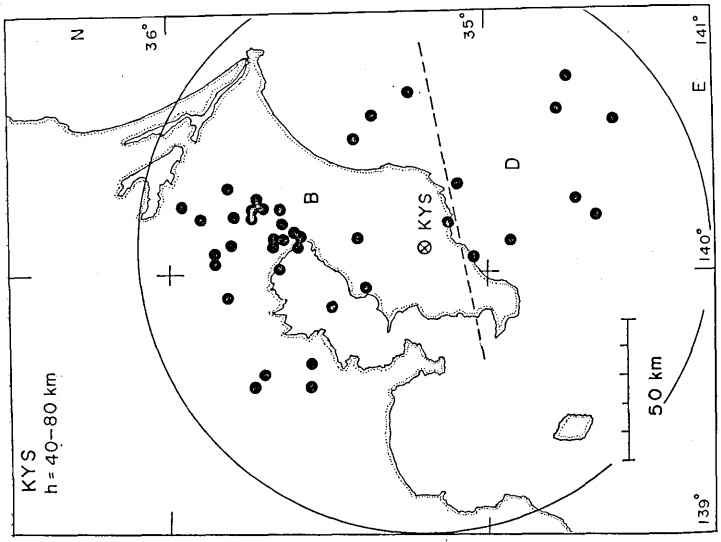

Fig. 3.3c. Epicenter locations of earthquakes used in the coda analysis at KYS. Explanation of the symbols is the same for those of Fig. 3.3a.

and a damping constant of 2 installed at the same station. This seismometer is useful for suppressing the saturation of amplifier by large low frequency components. The difference of displacement magnification of the two seismographs is shown in Table 2 for a comparison. In spite of the different site effect on the absolute amplitude of coda waves, the amplitude decays in a regular way as a function of lapse time measured from the origin time.

The analysis of coda waves is done through the following procedures as given by AKI and CHOUET (1975). The smoothed envelopes of the trace amplitudes (peak-to-peak) are measured directly from the chart records for each frequency band. Samples were taken every 2.4 sec for smaller events and every 4.8 sec for larger events lasting less than 160 sec after the origin time. Final reading for each trace was determined at a point where the signal-to-noise ratio falls to below 3. The noise levels were compared before and after for each event on all traces. An initial point for the measurement of coda amplitudes on a seismogram was arbitrarily chosen as a point, where the seismic signal starts to decay in a regular manner after the S wave arrivals.

Figs. 3.3a, -b, -c and -d show the spatial distribution of earthquake epicenters used at four stations. Most of these events occurred within 100 km at each station. According to the properties of attenuation and source spectrum obtained from S waves (TSUJIURA, 1973a), the Kanto district is separated locally into four areas as indicated by A, B, C and D. Broken lines show the boundary of these areas. Another two stations, OYM and HNG are used only for the comparison of coda excitation.

An example of the amplitude decay curves of coda waves which show very regular decrease for many earthquakes obtained at the TSK-A is shown in Fig. 3.4. Fig. 3.5 shows the same decay curves for the 24 Hz band obtained at the same station. The slope of the envelope depends on frequency, i.e., the higher the frequency the more rapid the decrease with the time. From these curves, the common curve indicated by a dashed line can be obtained by considering simultaneously all the events recorded on a given channel.

Similar amplitude decay curves including the different frequency bands are obtained at four stations. The equation shown in the figures will be explained later.

Another important fact about coda waves is that the time-dependence of coda decay is independent of the earthquake magnitude as suggested by AKI (1969). An example of the records for the events with magnitudes of 4.8 and 3.9 is shown in Fig. 3.6. These records were obtained by the seismographs with magnifications different by a factor of eight at the DDR station. The amplitude decay of the two events is quite similar

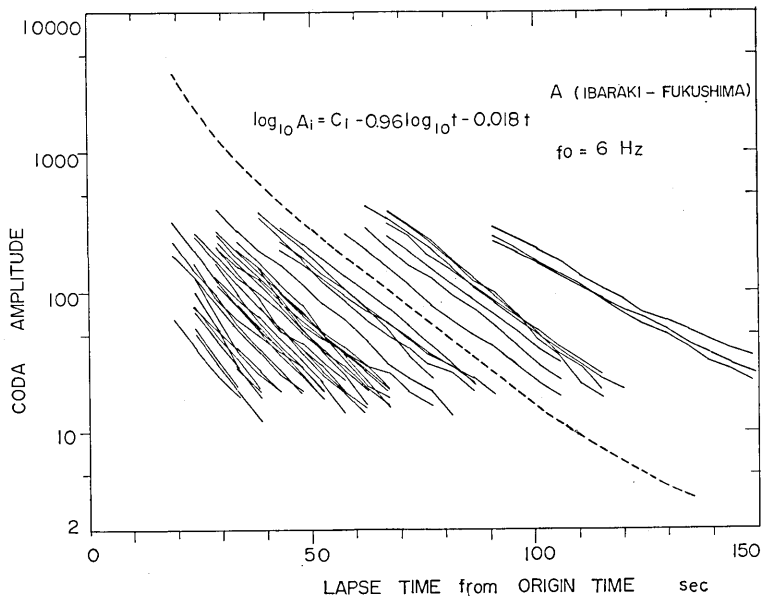

Fig. 3.4. Amplitude decay traces of coda waves measured at 6 Hz from earthquakes in the A area observed at TSK. The dashed line represents a common curve obtained by considering simultaneously all the events, and represents the function $\log_{10} A_i = C_i - 0.96 \log_{10} t - 0.018t$ obtained by fitting a common curve (see text for explanation of symbols and procedure).

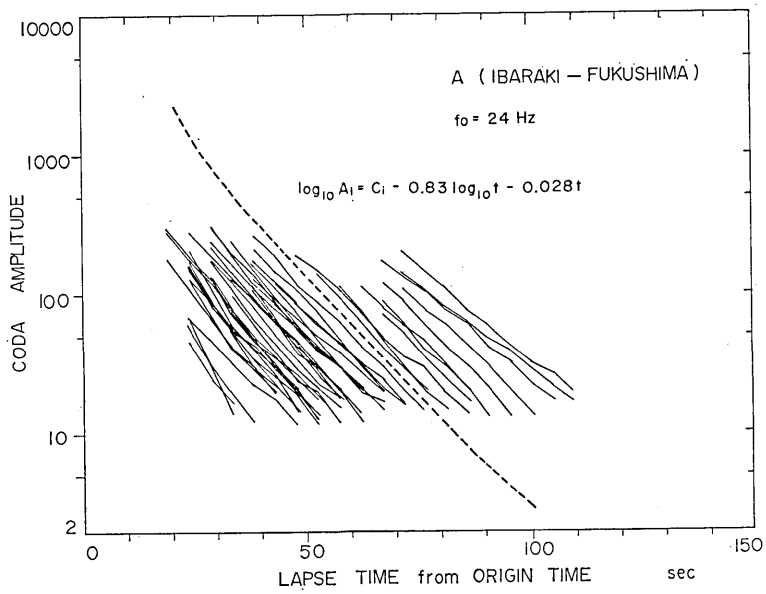

Fig. 3.5. Amplitude decay traces of coda waves measured at 24 Hz from earthquakes in the A area observed at TSK. The dashed line represents the function $\log_{10} A_i = C_i - 0.83 \log_{10} t - 0.028t$. Explanation of the symbols is the same for those of Fig. 3.4.

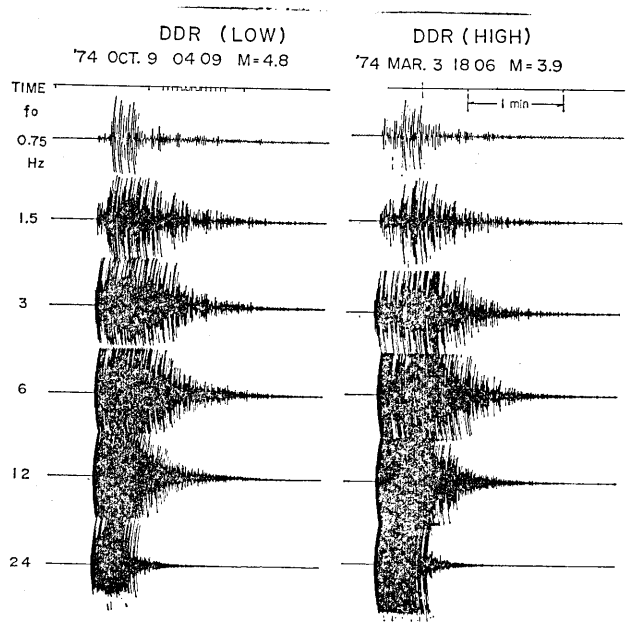

Fig. 3.6. An example of the filtered seismograms of two events with magnitudes of 4.8 and 3.9 obtained by seismographs with different magnification at DDR. Note similar coda decay for the same frequency bands of two events. The frequency from 0.75 to 24 Hz represents the center frequency (f_0) for each band-pass filter.

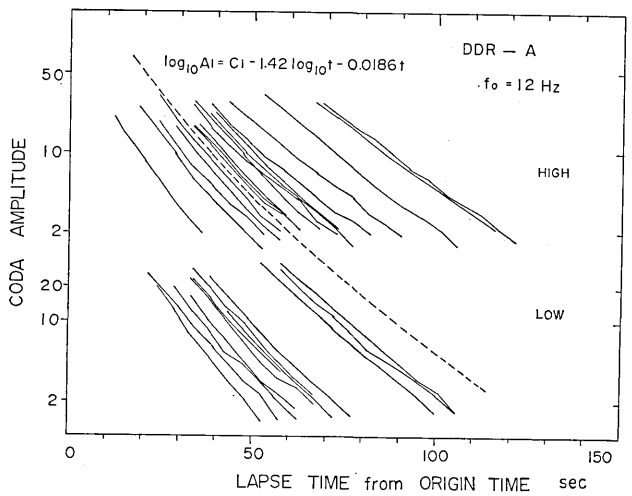

Fig. 3.7. Amplitude decay traces of coda waves at 12 Hz obtained by seismographs with different magnification at DDR. The upper and lower traces represent the results of high and low magnification seismographs, respectively. Explanation of the other symbols is the same for those of Fig. 3.4.

for all the frequency bands. Fig. 3.7 shows the coda decay curves for the 12 Hz band for many earthquakes obtained at the same station. Upper and lower lines indicate the results of high and low magnification seismograph, respectively. It is clearly seen that the time-dependence of coda amplitudes is independent on the magnitude of the earthquake.

A quantitative analysis of coda waves by the single scattering theory as well as the diffusion theory has been made by AKI and CHOUET (1975), who suggested that the coda amplitude $A(\omega|t)$ takes the following simple form as a function of time measured from the origin time;

$$\log_{10} A(\omega|t) = C(\omega) - a \log_{10} t - bt \tag{3.1}$$

where $C(\omega)=\log_{10} c(\omega)$, and $c(\omega)$ represents the source term at a frequency ω and it's related to the source factor of coda $S(\omega)$ by the relation

$$c(\omega) = 2[2S(\omega)\Delta f]^{1/2} \tag{3.2}$$

where Δf is the bandwidth of the filter on the particular channel considered, a is a constant that depends on the geometrical spreading with $a=0.5$ for surface waves and $a=1$ for body waves, and b is related to the quality factor Q by the relation

$$b = (\log_{10} e)\pi f/Q. \tag{3.3}$$

To separate the effects of source factors, geometrical spreading and attenuation in coda data, we shall use the least square method. Each channel output was treated separately, and the least square fits were obtained with the formula (3.1) for the dashed line obtained by taking all the events into consideration simultaneously. In obtaining the least square solution, two values of a, namely 1 and 0.5 are assumed as the constants of geometrical spreading, corresponding to body and surface waves, respectively.

As shown in Figs. 3.4, 3.5 and 3.7 the decay of coda amplitudes are very regular for many events, and the decay curve of each event can be shifted vertically to agree with the dashed curve within the errors of 20 %. The decay curve at high frequencies for deeper events ($h>100$ km), however, is somewhat different from those of shallower events ($h<80$ km), and it indicates slower rate of decreasing with time. Separate analysis therefore is made for the event above and below the source depth of 90 km.

Factors a and b computed by the use of Eq. (3.1) are summarized in Tables 3 and 4. The values computed for the factor a (Table 3) shows some deviation (0.3—2.3), because the value of a is very sensitive to the coda amplitude for small t. Our measurement of early coda is somewhat

Table 3. Values of the coefficient a in equation (3.1) obtained from the least square computation. f: frequency in hertz, *: deeper event (h=100−160 km).

Event Group	f=0.75	f=1.5	f=3.0	f=6.0	f=12.0	f=24.0
TSK—A	1.04	1.36	1.13	0.96	0.98	0.83
TSK—B	1.00	1.45	1.58	1.10	1.09	1.06
TSK—A, B*	—	0.62	1.52	1.94	2.04	2.31
DDR—A	1.21	0.76	0.73	1.37	1.42	1.31
DDR—B	—	0.75	1.26	0.80	1.13	0.31
KYS—B	0.98	0.70	1.41	1.60	1.00	0.32
IWT—A, B	0.41	0.45	0.87	1.35	1.34	1.47

Table 4a. Values of the coefficient b in equation (3.1) obtained from the least square computation with the factor a in (3.1) being free. f: frequency in hertz, *: deeper event (h=100−160 km).

Event Group	f=0.75	f=1.5	f=3.0	f=6.0	f=12.0	f=24.0
TSK—A	0.0055	0.0095	0.0160	0.0181	0.0226	0.0276
TSK—B	0.0055	0.0098	0.0155	0.0191	0.0202	0.0220
TSK—A, B*	—	0.0109	0.0095	0.0119	0.0110	0.0125
DDR—A	0.0067	0.0113	0.0161	0.0149	0.0186	0.0228
DDR—B	—	0.0127	0.0134	0.0158	0.0190	0.0307
KYS—B	0.0041	0.0080	0.0110	0.0151	0.0204	0.0372
IWT—A,B	0.0085	0.0121	0.0133	0.0125	0.0155	0.0180

Table 4b. Values of the coefficient b in (3.1) obtained from the least square computation with the factor a in (3.1) assumed to be 1. f: frequency in hertz, *: deeper event (h=100−160 km).

Event Group	f=0.75	f=1.5	f=3.0	f=6.0	f=12.0	f=24.0
TSK—A	0.0056	0.0116	0.0173	0.0197	0.0223	0.0256
TSK—B	0.0055	0.0117	0.0197	0.0199	0.0211	0.0219
TSK—A, B*	—	0.0083	0.0124	0.0174	0.0180	0.0190
DDR—A	0.0077	0.0096	0.0143	0.0171	0.0215	0.0259
DDR—B	—	0.0107	0.0148	0.0163	0.0175	0.0231
KYS—B	0.0038	0.0060	0.0125	0.0193	0.0202	0.0294
IWT—A, B	0.0046	0.0077	0.0124	0.0142	0.0176	0.0173

Table 4c. Values of the coefficient b in (3.1) obtained from the least square computation with the factor a in (3.1) assumed to be 0.5. f: frequency in hertz, *: deeper event (h=100−160 km).

Event Group	f=0.75	f=1.5	f=3.0	f=6.0	f=12.0	f=24.0
TSK—A	0.0089	0.0149	0.0208	0.0216	0.0260	0.0302
TSK—B	0.0088	0.0152	0.0233	0.0235	0.0247	0.0256
TSK—A, B*	—	0.0114	0.0153	0.0206	0.0218	0.0226
DDR—A	0.0112	0.0131	0.0178	0.0205	0.0253	0.0310
DDR—B	—	0.0137	0.0180	0.0194	0.0210	0.0276
KYS—B	0.0063	0.0089	0.0155	0.0226	0.0243	0.0343
IWT—A, B	0.0076	0.0107	0.0153	0.0174	0.0210	0.0212

uncertain since saturation occurrs on some of the recorded events, and the beginning of coda amplitude is not always well-defined. In addition, the coda amplitude at time shorter than 14 sec cannot be obtained since no earthquakes have occurred at the depth shallower than about 40 km. However, the estimate for b (Tables 4a, 4b and 4c) is relatively insensitive to the uncertainty in the estimate of a, because most of the coda lengths are controlled by bt (see Fig. 3.4). We shall study the b value which is related to the quality factor Q by Eq. (3.3).

4. Attenuation properties of coda waves

Using the method described in preceding section, and from the value of b (Tables 4a, 4b and 4c) a value of the quality factor Q of coda waves was calculated for each frequency. The value of Q against the frequency determined at TSK with two depth ranges and the other three stations of DDR, KYS and IWT are summarized in Figs. 4.1a and 4.1b. The marks of A and B attached to the station refer to the groups of events shown in Figs. 3.3a–3.3d. These Q values represent an average value of the attenuation properties over the area encompassed by the coda waves from many different local earthquakes for each area.

The estimated Q values depend on frequency, increasing with frequency. The Q value at about 1 Hz is relatively low, about 200, and at a high frequency of about 20 Hz it reaches 1500. This tendency is commonly observed at all the stations. The difference of Q between the areas A and B at TSK is not detectable, although there exists a clear difference of Q_β for S waves at a factor of 2.5 as will be described in section 6. This result suggests that the coda decay characteristics are independent of the epicenter location. However, close scrutiny of these

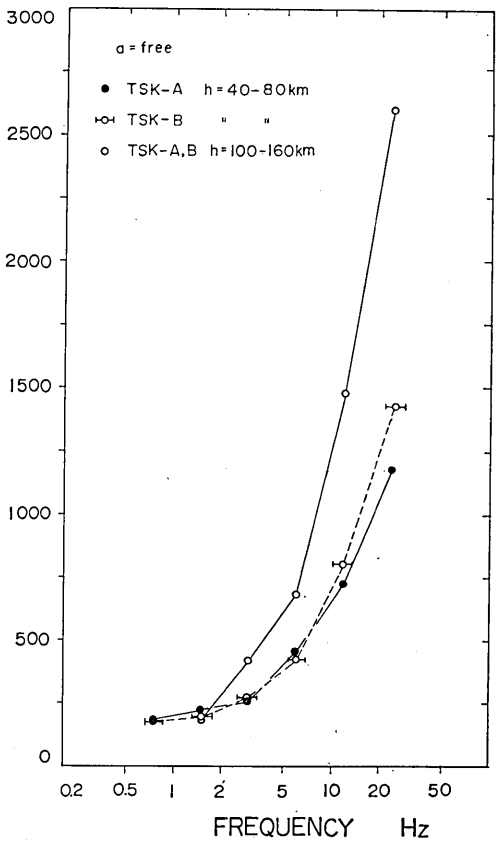

Fig. 4.1a. Q values in the range of 0.75–24 Hz derived from the analysis of coda waves observed at TSK. No constraint of the spreading factor is made for the computation (a=free). Closed circles and open circles with error bars represent Q values derived from the earthquakes with source depths (h) of between 40–80 km in the areas of A and B, respectively. Open circles represent Q values derived from the earthquakes with source depths of between 100–160km.

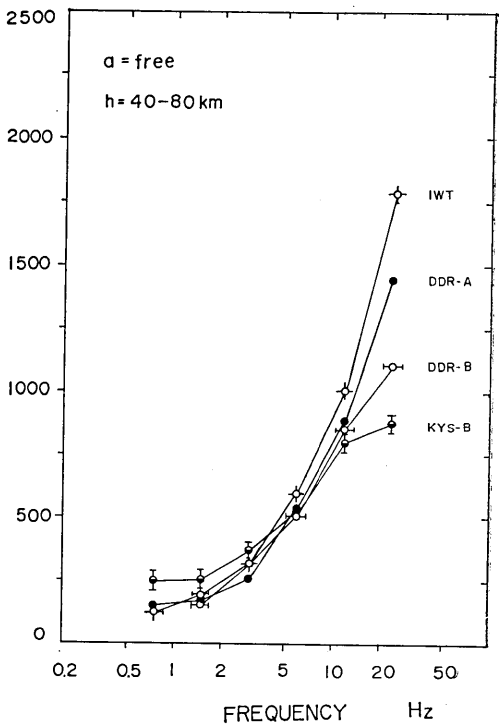

Fig. 4.1b. Local variations of Q in the range of 0.75–24 Hz derived from the analysis of coda waves observed at IWT, DDR-A, -B and KYS-B, respectively. No constraint of the spreading factor is made for the computation (a=free).

figures shows that there are local differences of the Q values over a factor of 2 from station to station. The Q value for high frequencies at KYS is relatively low, and that of DDR is intermediate between IWT and KYS. On the other hand, in the lower frequency range, KYS gives a maximum value. The local differences of Q obtained here correlate to the geological setting of the station site. This effect will be discussed further in section 5.

The value of Q for deeper events ($h=100-160$ km) obtained at TSK indicates the highest value at high frequencies in contrast to those of shallower events ($h=40-80$ km), and the difference amounts to more than a factor of 2 at 24 Hz. But the difference diminishes with decreasing frequency, and at about 1 Hz there is no difference for the events of 40−160 km.

The parameter a has little effect on the determination of Q. Fig. 4.2 shows the Q values obtained at TSK, with a different assumption of the spreading factor a. Open circles and with two type error bars, and closed

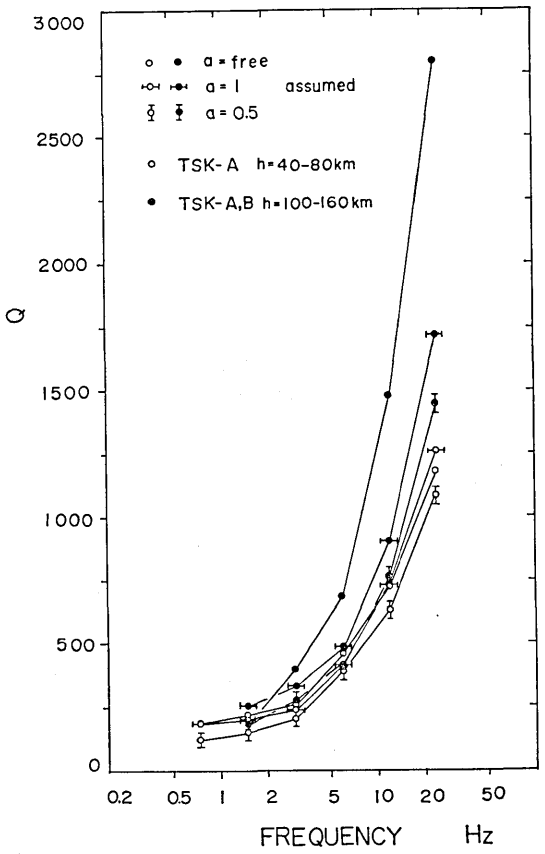

Fig. 4.2. Q values in the range of 0.75−24 Hz derived from the analysis of coda waves of earthquakes observed at TSK, with different assumptions of the spreading factor. Open circles and with two types of error bars, and the same symbols with closed circles refer to the assumptions of no constraint (a=free), body wave scattering ($a=1$) and surface wave scattering ($a=0.5$). Open and closed circles represent Q values derived from earthquakes with source depths (h) of between 40−80 km, and 100−160 km, respectively.

circles and with the same symbols refer to the assumption of no constraint (a=free), body wave scattering (a=1) and surface wave scattering (a=0.5). Open and closed circles represent the Q values derived from earthquakes with source depths (h) of between 40−80 km and 100−160 km, respectively. The Q value derived from shallower events at TSK varies from 150−200 at 0.75 Hz to 1100−1250 at 24 Hz. On the other hand, the Q from deeper events shows relatively larger deviation at high frequency (1500−2800 at 24 Hz). This behavior is also understandable, because as mentioned earlier, factor a is very sensitive to the coda amplitude for small t, and the beginning of the measurement of coda from deep sources becomes later in time. Fig. 4.3 shows the Q values obtained at four stations where the spreading factor a was fixed at 1. The quality factor again shows consistently low at 1 Hz and high at higher frequencies.

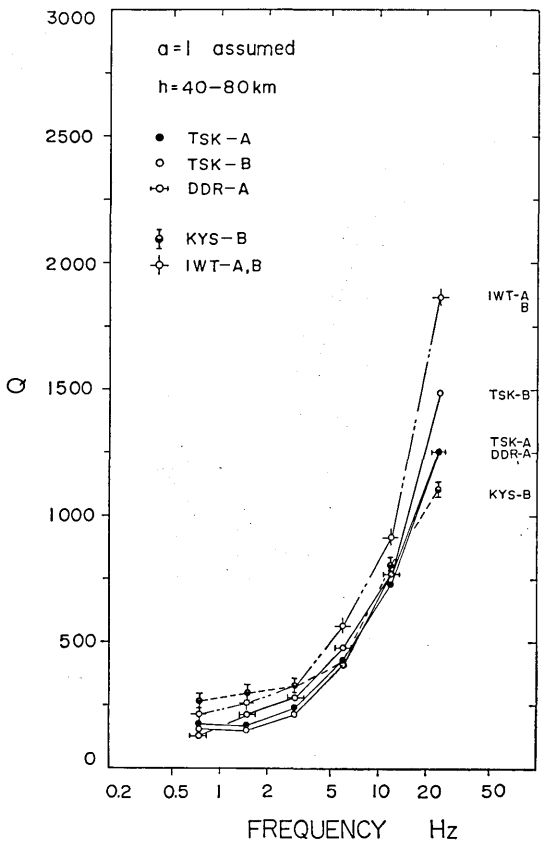

Fig. 4.3. Q values in the range of 0.75−24 Hz derived from the analysis of coda waves observed at TSK-A, -B, DDR-A, KYS-B and IWT. The body wave scattering (a=1) is assumed as the spreading factor for the computation.

The high Q at high frequencies can be seen directly from the filtered records. For example, if the Q obtained at 1 Hz was to be applicable at 24 Hz also, it is expected that the signal of the 24 Hz band will disappear in a matter of a few seconds. The existence of coda waves of this frequency for more than 100 sec (see Fig. 3.5) clearly indicates that the Q of coda waves depends on frequency.

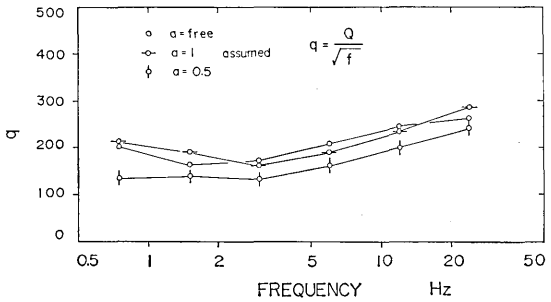

Fig. 4.4. q values in the form $Q=qf^{1/2}$ for averaged Q at four stations against the frequency. Different choices of the spreading factor a; a=free, a=1 and a=0.5 is assumed for the computation.

A similar result on frequency-dependence of Q for coda waves has been reported in other seismic areas (AKI and CHOUET, 1975; CHOUET, 1976; RAUTIAN and KHALTURIN, 1976). Rautian and Khalturin pointed out that the dependence of Q on frequency takes the form of $Q=qf^{1/2}$, and the coefficient q for the Garm region, Tadjikistan is approximately equal to 270 for the frequency range from 1.25 Hz to 18 Hz. Fig. 4.4 shows the q values for averaged Q at four stations for the various choices of the geometrical spreading factor. The value of q is relatively constant in the frequency range from 0.75 Hz to 24 Hz within the values of 165−265 for a=free, 160−280 for a=1 and 135−240 for a=0.5, respectively. However, for coda waves, the increase in Q with frequency may not be due to an intrinsic frequency-dependence of Q. Aki and Chouet suggested that it may be observing the dependence of Q on depth for waves scattered from different parts of the earth's crust. In other words, the coda waves at about 1 Hz may be primarily composed of surface waves scattered from shallow low-Q heterogeneities and those at about 20 Hz are essentially backscattering body waves from the deep high-Q lithosphere. If such an explanation is applied equally to our area studied, it seems likely that the lowest Q for frequencies above 12 Hz at KYS may be due to relatively low-Q material composing most of the crust under the station. This is consistent with the result indicating the lowest detection capability for P-waves of teleseismic events among the stations concerned (MIYAMURA

and YAMADA, 1973). The largest Q for about 1 Hz at KYS therefore apparently may be due to the existence of a thin surface layer with high-Q under the station. This effect will be further discussed in the next section.

5. Dependence of coda excitation on local geology

It has been well known that the seismograms of an earthquake, recorded at many stations on different geological formations, differ significantly from one station to another in their forms, amplitudes, periods and total durations. Numerous studies on this subject have been made by many seismologists since the beginning of modern seismology. Most of these studies suggested that for sites underlain by a layer of sediments, maximum ground amplitudes generally increased with thickness of the layer, and relatively larger amplitudes last several times as long as at those recorded on nearby bedrock.

Following AKI (1969), who showed a strong dependence of coda excitation on local geology, we studied the effect of local geologic structure on coda waves observed at the six stations located on a variety of formations, including granite, crystalline schist, andesite, sandstone and loam layer (Fig. 2.1 and Table 1). The method of interpreting coda waves is the same as given in previous section. The coda spectra from more than

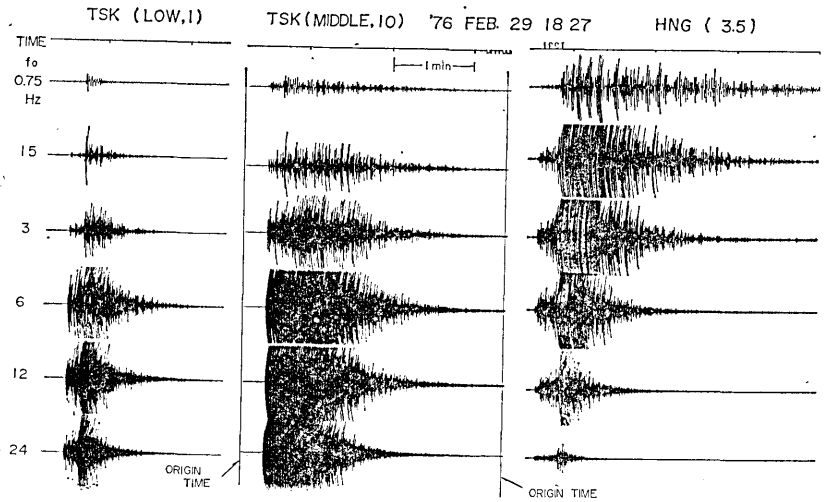

Fig. 5.1. Typical example represents the difference of coda excitation. The filtered seismograms of left, middle and right hand side correspond to those at TSK with two kinds of magnification and at HNG. Relative differences of magnification are 1:10:3.5. f_0 indicates the center frequency of band-pass filters with one octave bandwidth, (see Fig. 2.3).

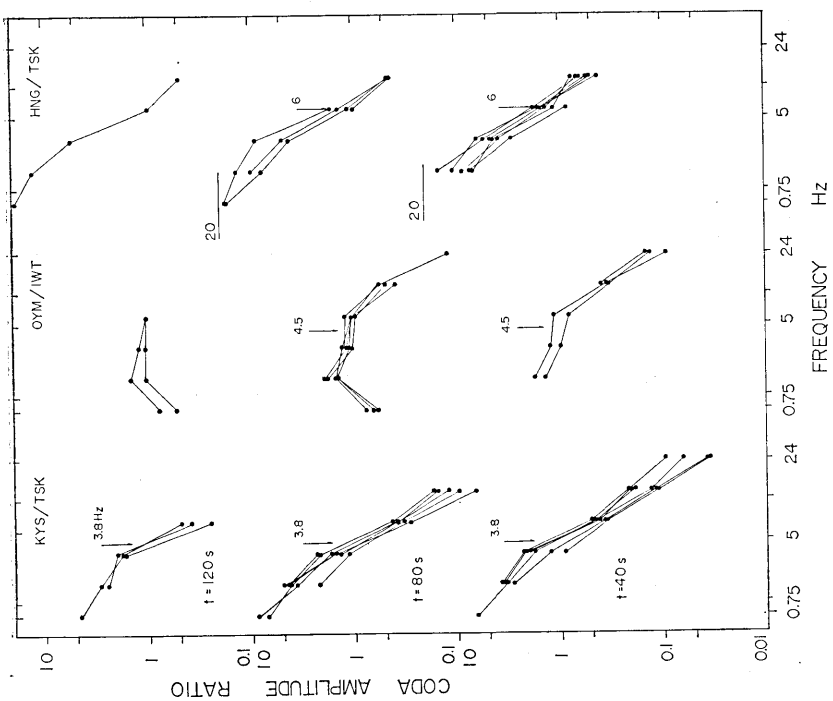

Fig. 5.2b. Amplitude ratio of coda waves for pairs of stations as a function of lapse time measured from the origin time. Explanation of the symbols is the same for those of Fig. 5.2a.

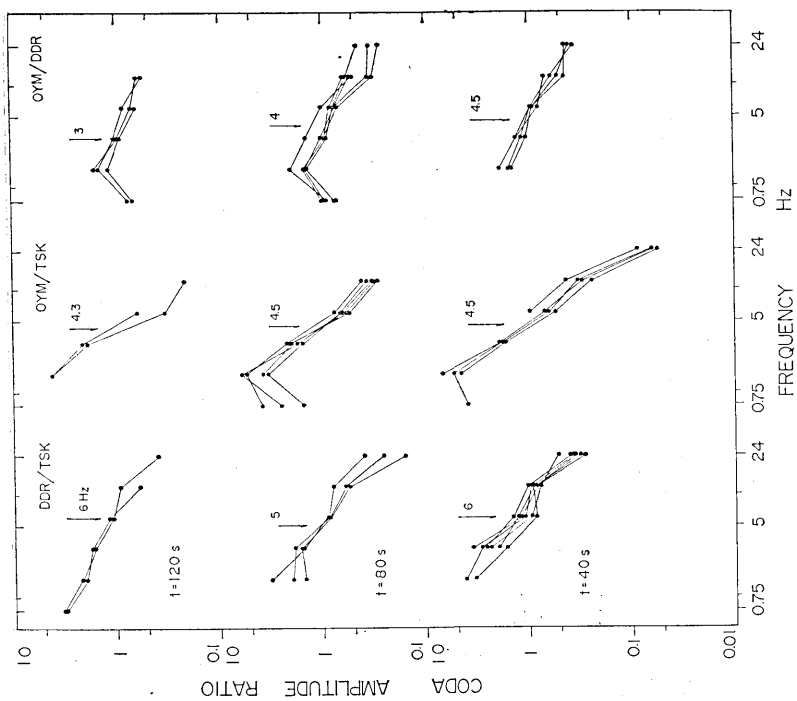

Fig. 5.2a. Amplitude ratio of coda waves for pairs of stations as a function of lapse time measured from the origin time. The ratio of bottom, center and top groups corresponds to the result for lapse time of 40, 80 and 120 sec, respectively.

ten earthquakes with epicenters distributed over the wide azimuth around a station are used in the analysis.

There is a strong amplitude-frequency dependence of coda excitation among the stations. Fig. 5.1 shows the filtered records of the same earthquake observed at TSK with two kinds of magnification and at Hongo (HNG), where the seismometer is installed in the basement of the Earthquake Research Institute building. The ground formation of TSK and HNG consists of granitic rocks and the Kanto loam layer, respectively. A relative difference of the magnification between the filtered records is 1 : 10 : 3.5 as indicated in parenthesis, respectively. As is described by many authors mentioned earlier, the periods of corresponding waves

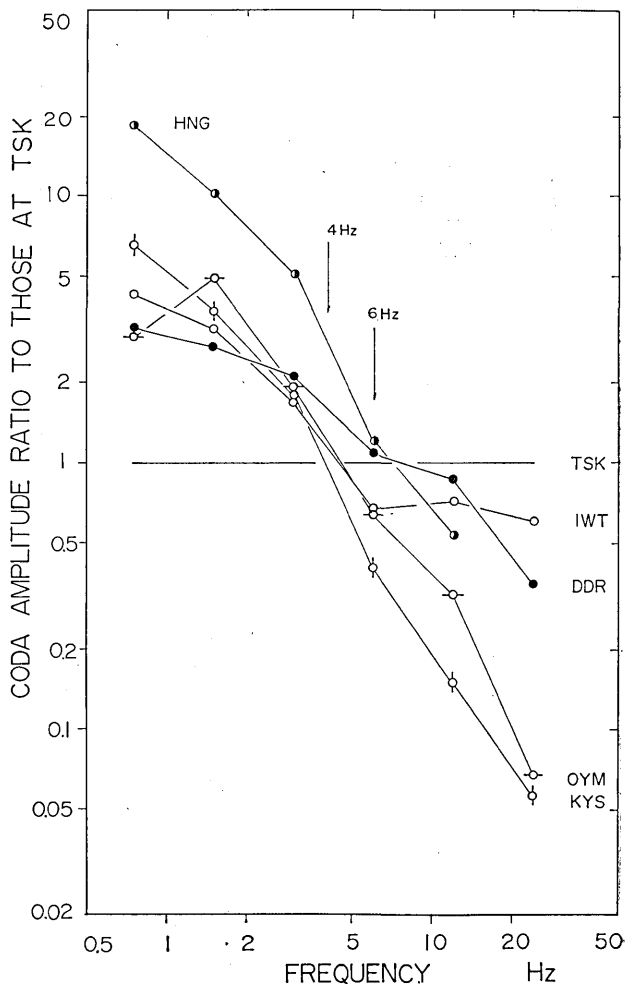

Fig. 5.3. Average amplitude ratios based on those at TSK.

may differ significantly at various sites with different geology. Waves having relatively short periods may be emphasized by ground conditions at some sites (e.g., TSK), and waves having appreciably longer periods at others (e.g., HNG). Consequently, the amplitude ratio obtained from different formations depends on frequency.

We measured a smoothed amplitude of coda waves for each frequency band as a function of lapse time measured from the origin time. Figs. 5.2a and 5.2b show the amplitude ratio of coda waves recorded at six pairs of stations for the lapse times of 40, 80 and 120 sec. There is a clear dependence of amplitude ratio with frequency, roughly independent of the lapse time. The arrow shows the frequency at which the amplitude is the same for the station pair. From these results the average amplitude ratios based on those at TSK are summarized in Fig. 5.3. We found that the amplitude ratios are different by a maximum factor of 20 between the stations. For example, KYS, OYM and HNG indicate consistently greater amplitudes, on the average, 6-20 times at low frequencies and smaller amplitudes about 0.05-0.1 times at the highest frequency compared with those of TSK. Generally speaking, the sites which show greater values at low frequencies always indicate smaller values at high frequencies. The site factors at each station are summarized in Table 5 together with the local surface geology. Such differences of site factors may be expected for much longer period coda waves. Reproduction of original records is shown in Fig. 5.4 as the example obtained by the same type seismographs with a natural period of 10 sec installed at TSK and KYS.

Table 5. Site factor of coda excitation with frequency dependence at six stations in the Kanto district. f: frequency in hertz.

Station	Formation	f=0.75	f=1.5	f=3.0	f=6.0	f=12.0	f=24.0
TSK	Granite	1.0	1.0	1.0	1.0	1.0	1.0
DDR	Crystalline schist	3.2	2.7	2.1	1.07	0.85	0.36
IWT	Quartz porphyry	4.2	3.1	1.6	0.67	0.71	0.60
OYM	Andesite	2.9	4.9	1.9	0.63	0.32	0.07
KYS	Sandstone	5.6	3.6	1.7	0.41	0.15	0.05
HNG	Loam	18.3	10.0	5.0	1.2	0.54	<0.1

There is a remarkable correlation between the site factor and the local surface geology of station site. We found that the "soft formation" i.e., a sandstone and loam layer have a site factor with greater values at low frequencies and smaller values at high frequencies. In other

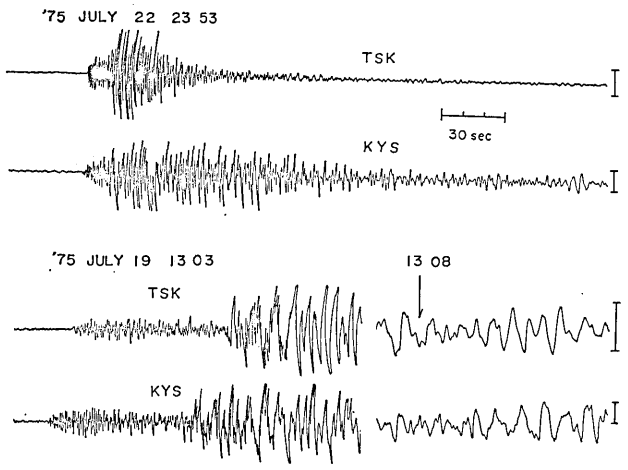

Fig. 5.4. Reproduction of original seismograms obtained by the medium-period seismograph (T_0=10 sec) at TSK and KYS. Note the difference of coda amplitudes. Error bars show the relative difference of magnification.

words "hard formations" such as granitic rocks have the smallest value at low frequencies and the greatest value at high frequencies. This result may be explained by the weak attenuation of granitic rocks and lack of heterogeneity or layering in hard formations. In contrast, soft formations consisting of many layers of different velocity will behave as a wave-guide to amplify low frequency waves. Consequently, it is expected that the Q estimated from coda waves should increase for these low frequency waves.

A recent investigation by SHIMA *et al.* (1975) gives the detailed underground structure in the metropolitan area of Tokyo, and the theoretical ground amplification characteristics at HNG have been computed by TANAKA *et al.* (1975). They suggested the existence of predominant frequencies within the range of 1 Hz−5 Hz at HNG. Our result at HNG is consistent with their results if we assume that the incident wave spectrum of bedrock (−2300 m) at HNG is the same as that of IWT which is located on the bedrock down to 3500 m from the ground surface (TAKAHASHI and HAMADA, 1975). A similar effect will be expected for other stations based on soft formations.

As is described above, the coda site factor depends on the local geology of the station site. In order to check if the same type rock will generate the same coda amplitude, or how the rock type relates to the body wave spectra, we shall make a comparison of the data observed at a small-aperture array of the seismographs. The station spacing for such an array analysis should be less than the wave length concerned.

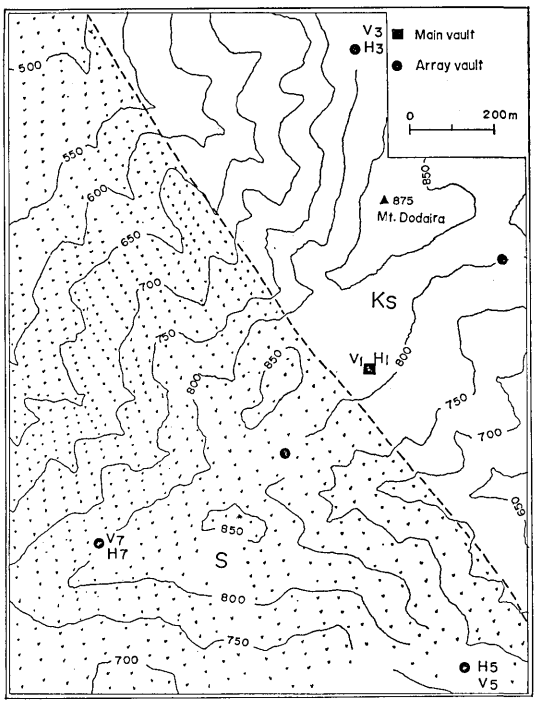

Fig. 5.5. Seismometer locations with local geology at the DDR array station. Dotted line indicates the boundary of the geologic formation. S: crystalline rocks, Ks: Kasayama group including slate, chert and schalstein rocks. V: vertical seismometer, H: horizontal seismometer.

Fig. 5.5 shows the location of array stations at DDR together with the local geology. The spectral comparison of coda- and *S*-waves are made for local earthquakes whose epicentral distances ranged between 40 and 120 km. In this case, the differences in radiation pattern and in the effect of the propagation path for each earthquake are negligible. The difference of the spectrum therefore can be treated as the effect of local geology beneath the station.

Fig. 5.6 shows the amplitude ratio of *S*- and coda-waves obtained by E-W component for the pair stations of H1/H5, H3/H5 and H7/H5 where the distance between the stations was 775 m, 1438m and 902m, respectively. The ratio for station pairs shows some frequency dependence. The closed lines show the average value of amplitude ratio for each frequency. The resonant frequency with relatively larger amplification appears within the band of 1.5-6 Hz. The site with maximum amplification, an average 3 times that of H5, is H1, and minimum, within 30% of that of H5, is H7 for *S* waves. This tendency is almost the same, within a factor of 30% for the ratio of coda waves which, however, indicates much less scattering

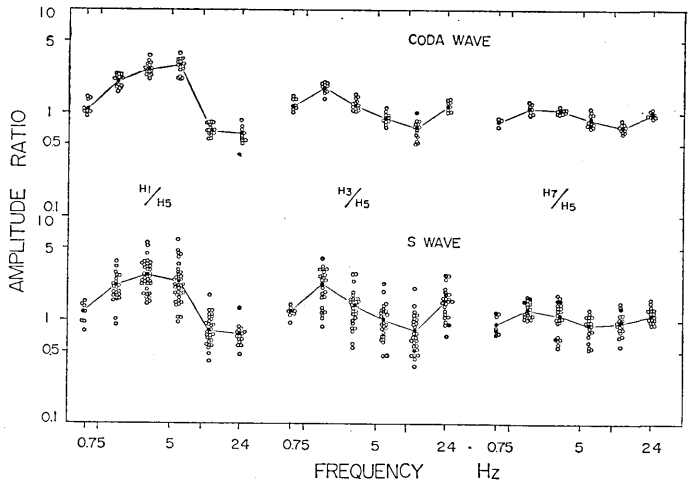

Fig. 5.6. Amplitude ratios of *S*- and coda waves for three station pairs within the DDR array in the frequency range from 0.75 to 24 Hz. Closed lines show the average amplitude ratio for each frequency.

at each frequency. Small deviation in the amplitude ratios for coda waves can be explained by Aki's assumption that coda waves are the superposition of the secondary waves generated by the heterogeneities distributed over a large area, and the amplitudes are insensitive to the local differences of the underground structure (AKI, 1969). The same tendency between coda and *S* wave ratios is also understandable if we assume the same velocity for both waves, because the resonance frequencies at a given station are given by the formula of $f=V(2i-1)/4H$ for $i=1, 2, 3\cdots$, where V is the wave velocity and H is the thickness of the inhomogeneous media under the station (e.g., TAKAHASI and HIRANO, 1941).

A similar comparison is made for *P* waves observed by vertical component. Fig. 5.7 shows the amplitude ratios of *P* waves observed by the same station pairs V1/V5, V3/V5 and V7/V5. The amplitude ratios depend

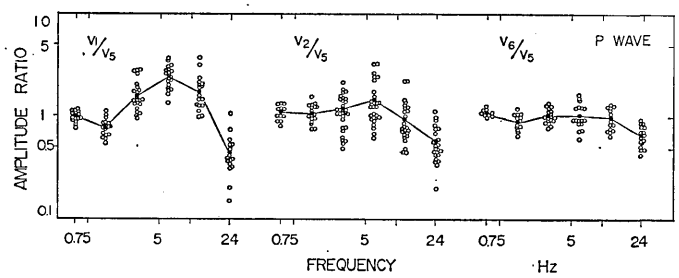

Fig. 5.7. Amplitude ratios of *P* waves for three station pairs within the DDR array in the frequency range from 0.75 to 24 Hz.

on frequency in the same way as those of S waves. However, the frequency of maximum amplification is shifted to the higher frequency range, 2-4 times that of S waves. This may be due to the difference of velocity between P and S waves.

As is shown in Fig. 5.5, the DDR seismometer array is located on different rocks. H5, H7 (V5, V7) are located on crystalline schist rocks (S), and H1, H3 (V1, V3) are located on Kasayama group rocks (Ks) including slate, chert and schalstein rocks. The difference of the spectral amplitudes therefore may be due to the different formations of station sites. The structure under the Kasayama group will be more complicated compared to the crystalline schist.

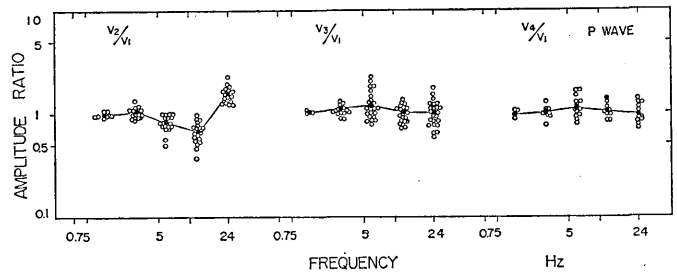

Fig. 5.8. Amplitude ratios of P waves for three station pairs within the TSK array in the frequency range from 1.5 to 24 Hz.

A similar array analysis was extended to TSK where granitic rocks are exposed at all the stations. Fig. 5.8 shows the amplitude ratio for P waves observed at three station pairs with about 300 m spacing. The amplitude ratios depend on frequency, within a range of maximum 50%. Thus, we may conclude that the difference of the site effect still remains even for the same geological formation. The spectral checking at several points around the station will be needed in order to know the geological effects for a specified station.

Studies on the spectral difference of body and coda wave excitation according to local geology will be important when the spectral data is used to determine the source parameter. The correction for the site factor as well as the effect of attenuation must be applied to the observed spectral data. Some site corrections dividing by a constant have been made for the determination of source spectra (AKI, 1969; THATCHER and HANKS, 1973; JOHNSON and MCEVILLY, 1974). However, our data show that the site factors are clearly frequency dependent. Thus, the site factor for a wide frequency band can be obtained from the spectral comparison of coda waves from local earthquakes.

6. Dependence of source spectra on earthquake magnitude

In order to study the dependence of seismic source spectra on earthquake magnitude, we shall use the spectral ratio of coda waves. Following AKI and CHOUET (1975), the ratio of coda power for two different earthquakes of $P_1(\omega|t)$ and $P_2(\omega|t)$ is equivalent to the ratio of source factor of $S_1(\omega)$ and $S_2(\omega)$ since the effect of propagation path is common for both sources, and can be written as

$$\frac{P_1(\omega|t)}{P_2(\omega|t)}=\frac{S_1(\omega)}{S_2(\omega)}. \tag{6.1}$$

The relative value of the source spectra for two different earthquakes can be determined from the ratio of the source factor of coda amplitude. As mentioned earlier, although the coda excitation depends on the local geology of the station site, the relative source factor determined at a given station for different earthquakes is unaffected by the local geology. However, a direct determination of source spectra is required for at least one of the earthquakes included in the data set in order to fix the absolute value of the source spectrum. The theory of far-field body waves generated by a dislocation source buried in an unbounded homogeneous elastic media will be applied to many of the smallest and nearest events. The data of TSK are used for this purpose since there is less site effect (Fig. 5.3), and this fact suggests the existence of relatively homogeneous media.

As is well known, earthquakes with source depths greater than 40 km are very active in the Kanto district. We shall make a scaling law of source spectra for these events. Aki and Chouet suggested that events of 40 km are too far away to be considered nearest events. However, there are no shallow events around TSK, and the source spectra vary according to source depth (TSUJIURA, 1969, 1972). Moreover, the dependence of the spectrum on the local geology of the station site is different for P and S waves, and the dependence for S waves is more similar to that of coda waves (see Figs. 5.6 and 5.7).

Some of the filtered records of these smallest and nearest earthquakes observed by the E-W component seismograph at TSK are shown in Fig. 6.1. For these smallest earthquakes with a magnitude of about 1.5 the high frequency bands centered at 48 and 96 Hz were added. Although the nearest earthquakes are more than 40 km away from TSK they occur directly beneath the station (e.g., TSUMURA, 1973). A small ratio of epicentral distance to source depth would be expected to suppress the contamination of surface waves as suggested by PEKERIS and LIFSON

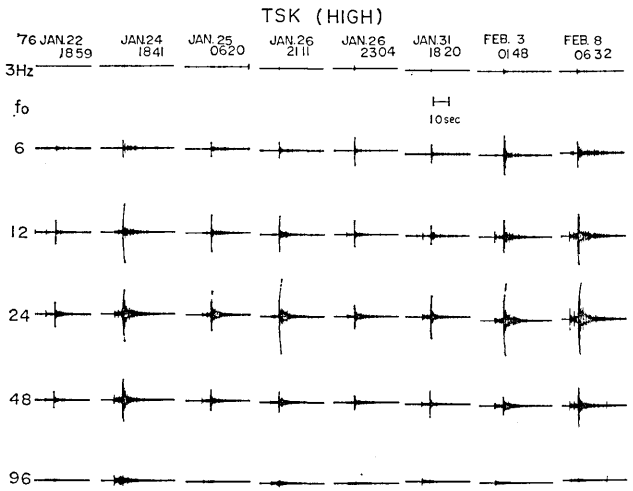

Fig. 6.1. Typical example of the filtered seismograms of the smallest and closest events at TSK. These events are used to determine the absolute level and spectral characteristics of earthquakes with magnitude around 1.5.

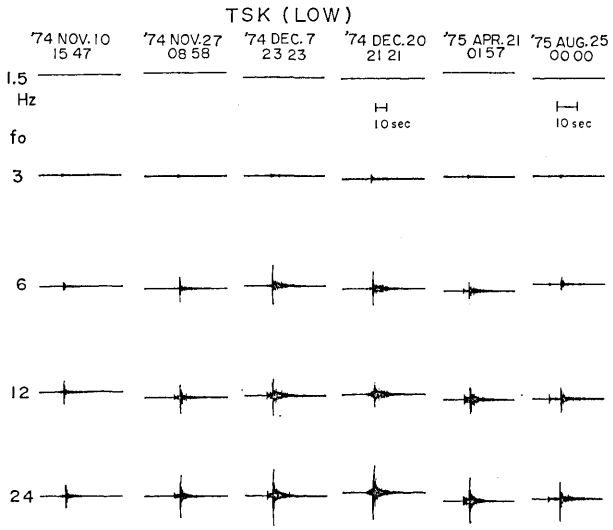

Fig. 6.2. Typical example of the filtered seismograms of about $M3.5$ earthquakes observed by the low magnification seismograph at TSK. Coda amplitude of the same event can be obtained more clearly by the high or middle magnification seismograph (see Fig. 3.1). These events are used to determine the absolute level and the spectral characteristics of $M3.5$ earthquakes, and to fix the absolute values of source factors of their coda waves.

(1957). A clear and simple S-wavelet can be seen for each band except the 96 Hz band. These records suggest the validity of applying the simple far-field solution. Fig. 6.2 shows records of larger events with a magnitude (M) about 3.5 observed by the low magnification seismograph at the same station (Fig. 2.2). The coda amplitudes of $M=3.5$ events are measured more precisely by the middle magnification seismograph (Figs. 2.2 and 3.1). From the combined data of the middle and low magnification seismographs the absolute value of the source factor of coda amplitudes for M 3.5 can be determined. The absolute values of source factors for greater earthquakes therefore are obtained by use of the source factors of coda amplitudes relative to that of the M3.5 event.

Following AKI and CHOUET (1975), the Fourier transform $F(\omega)$ of displacement due to far field S waves in an unbounded homogeneous elastic medium at a distance r from the source can be written as

$$F(\omega)=c(4\pi\rho\beta^3 r)^{-1}\dot{M}(\omega) \tag{6.2}$$

where c is a geometrical factor, ρ is the density, β is the shear-wave velocity and $\dot{M}(\omega)$ is the Fourier transform of the time derivative of seismic moment. For a band-pass signal with $|F(\omega)|=F$ (constant) in $\omega_2<|\omega|<\omega_1$, $|F(\omega)|=0$ otherwise, and $\phi(\omega)=0$ for all ω, the corresponding signal $f(t)$ is written as

$$\begin{aligned} f(t)&=1/2\pi\int_{-\omega_1}^{-\omega_2}Fe^{i\omega t}d\omega+1/2\pi\int_{\omega_2}^{\omega_1}Fe^{i\omega t}d\omega \\ &=2Ff_1\frac{\sin\omega_1 t}{\omega_1 t}-2Ff_2\frac{\sin\omega_2 t}{\omega_2 t} \end{aligned} \tag{6.3}$$

where $f_2=\omega_2/2\pi$ and $f_1=\omega_1/2\pi$. The maximum amplitude is at $t=0$ and is equal to

$$f_m=2F(f_1-f_2)=2F\Delta f \tag{6.4}$$

where Δf is the bandwidth of the filter. Thus for a rough approximation the amplitude of a wavelet is the product of its amplitude spectral density and twice the bandwidth. From the known bandwidth of the band-pass filter and the maximum amplitude of the S wave measured on each frequency, the amplitude spectral density $|F(\omega)|$ of the S wave is estimated by averaging over many small events with magnitudes of 1.5 ± 0.3 and 3.5 ± 0.3 as shown in Figs. 6.1 and 6.2.

In order to correct the resulting source spectrum for attenuation, we studied the amplitude ratio for two frequency bands of S waves for many earthquakes as a function of travel time. Fig. 6.3 shows the amplitude ratio for two frequency bands centered at 24 Hz and 6 Hz

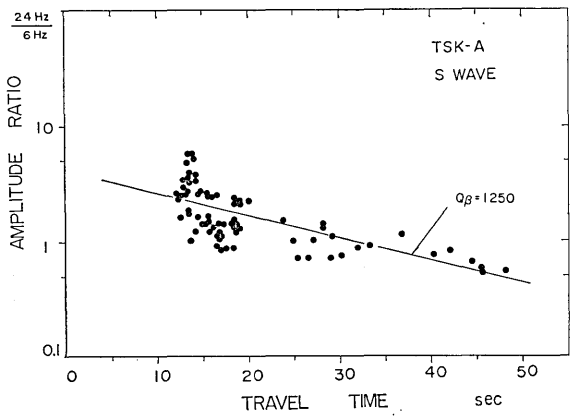

Fig. 6.3. Relation between the amplitude ratio of 24 Hz/6 Hz for S waves and the travel time for the earthquakes of TSK-A. Solid line represents the attenuation of S waves in the TSK-A area (see text for procedure).

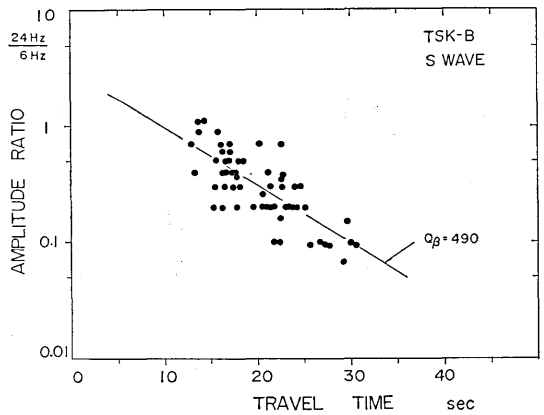

Fig. 6.4. Relation between the amplitude ratio of 24 Hz/6 Hz for S waves and the travel time for the earthquakes of TSK-B. Solid line represents the attenuation of S waves in the TSK-B area (see text for procedure).

of S waves against the travel time in the TSK-A area. Fig. 6.4 shows the same result for the TSK-B area. The areas A and B are the same as defined previously in the case of coda analysis. The magnitude and the source depth of these events range from 2.5 to 3.0 and from 40 km to 70 km, respectively. If the source spectrum does not change significantly within the ranges of magnitude and source depth concerned here, the dependence of observed amplitude ratio on travel time can be taken as the effect of attenuation on the S waves (TSUJIURA, 1966). Let R_1 and

R_2 be the maximum amplitude of S waves at two frequencies for f_1 and f_2, respectively, and t is the travel time. The amplitude ratio R_1/R_2 is written as

$$\log_{10} R_1/R_2 = (\log_{10} e)\pi t(f_1 - f_2)/Q_\beta. \tag{6.5}$$

Thus, an average Q_β over many different paths is obtained by the use of the least squares method. The average Q_β for the TSK-A and -B areas are 1250 and 490, respectively. These values refer to each area covered by direct wave paths for the S waves from earthquake foci between 40 and 70 km for both areas. Some of the scatter in the data may be accounted for by the difference in source spectra for individual earthquakes.

Seismic waves traveling from earthquakes in the area A to TSK pass through an inclined seismic zone with weak attenuation (TSUJIURA, 1972). BARAZANGI and ISACKS (1971) suggested that the average Q_β is of an order of 10^3 in the dipping seismic zone of Tonga region. Moreover the Q structure in the interpretation of coda waves observed at the TSK-A consists of low-Q, around 200 in the shallower part of the crust and high-Q, around 2500 in the deeper lithosphere. The evaluated value of Q_β as large as 1250 is not unreasonable as an average over the depth range from 0 to 70 km. A value of Q_β for the TSK-B is relatively low, about 500. A low value of Q_β for the TKS-B is consistent with the result of the previous study (TSUJIURA, 1973a).

To correct the effects of attenuation, spectral amplitudes $F(\omega)$ are multiplied by an exponential term $\exp(-\pi ft/Q_\beta)$, where t is the travel time of S wave, f is the frequency and Q_β is the quality factor obtained above. Although small site effects exist within the TSK array (Fig. 5.8), our station (V1) used in the coda analysis is the smallest (within 30%). No site correction is made for the determination of source spectra. Thus the source spectra of the smallest events are obtained. Fig. 6.5a shows the average source spectrum for three sets of these earthquakes as indicated in the previous Figures 6.1 and 6.2. The upper dashed curve for each set shows the source spectrum corrected by a value of Q_β 1200, and their average travel time 14 sec. The number of events (N) used and their average magnitude (M) are attached to each curve. These earthquakes occurred around TSK in northern part of 36°N (TSK-A), and their source depths are between 40 and 50 km. Q_β of 1100 and 1300 are examined for the smallest events in order to see the deviation of the source spectrum. No significant difference of the spectrum can be seen except in the rate of spectral amplitude decay at high frequencies. The amplitude of the 96 Hz band is not considered to determine the decay characteristics, because the poor signal-to-noise ratio and uncertainty in

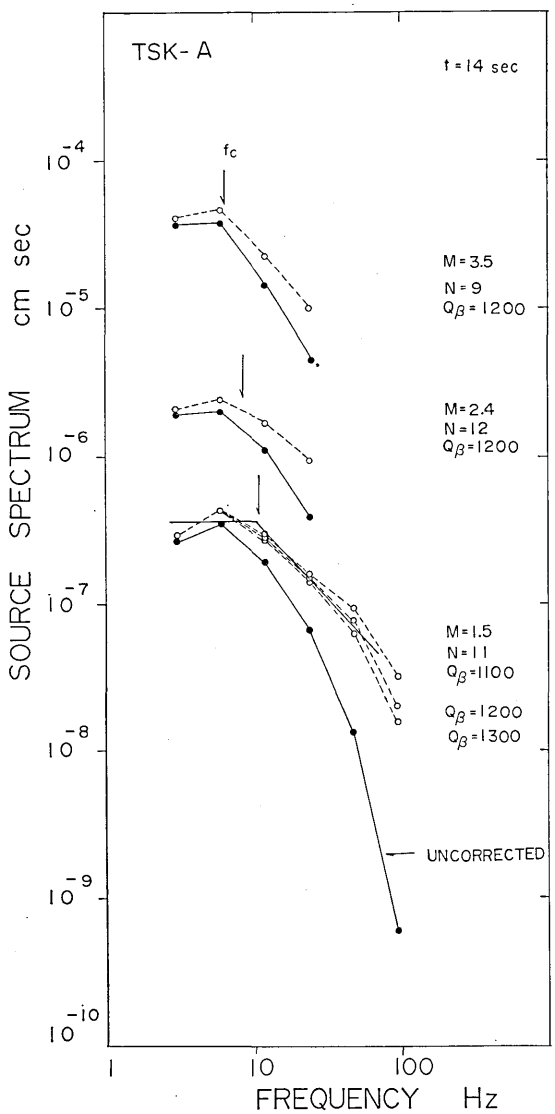

Fig. 6.5a. Average source spectra, corrected for attenuation, of the $M1.5$, $M2.4$ and $M3.5$ earthquakes obtained at TSK-A. N: number of shocks used, f_c: corner frequency.

the measurement of the amplitude at this frequency cause too much variability in the estimation of spectral decay. The spectral curve through the data corrected for Q_β 1200 is finally determined. Since our data consist of the band-pass filter records, a constant long-period level (Ω_0), a spectral corner frequency f_c and a high frequency spectral asymptote f^{-k} are not determined uniquely, therefore these values are approximated

by reducing them to two straight lines that intersect at the corner frequency. The approximated spectrum indicated by a closed line shows a corner frequency f_c at 12 Hz for the magnitude of 1.5, and decays with frequency in proportion to f^{-1} beyond the corner frequency. As the magnitude increases, the value of f_c decreases slightly, and is about 6 Hz for the magnitude of 3.5. The decay at high frequency for $M3.5$ event has a slightly steeper slope -2.

Similar source spectra corrected by $Q_\beta=500$, and $t=15.5$ sec for two sets of event groups that occurred about 25 km south from TSK (TSK-B) are shown in Fig. 6.5b. The source depth of these events ranges from 40 to 60 km, with an average of 52 km. Although the corner frequency is similar to that of TSK-A, the high frequency fall-off characteristics indicate a slightly steeper slope -2 for similar magnitudes ($M=2.4$), and a yet steeper slope of roughly -3 for larger earthquakes ($M=3.5$). It is

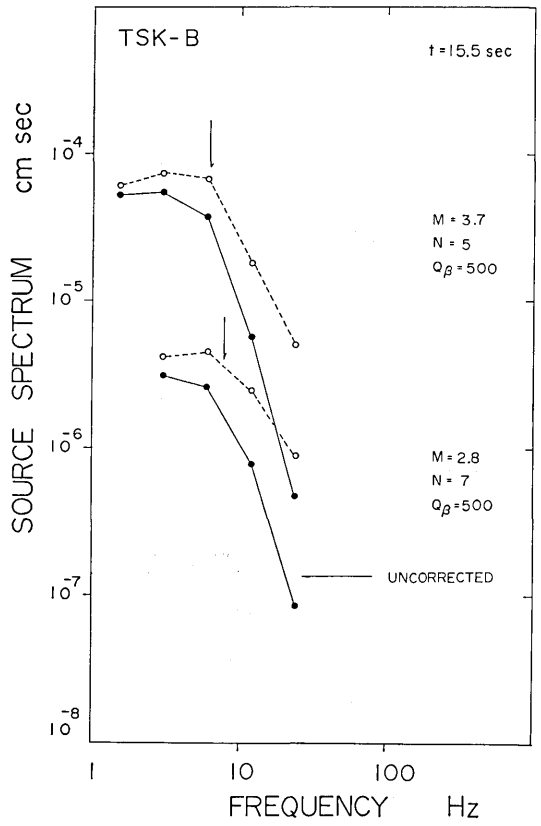

Fig. 6.5b. Average source spectra, corrected for attenuation, of the M 2.8 and M 3.7 earthquakes obtained at TSK-B. N: number of shocks used.

interesting to note that the steepness of the high frequency asymptote increases with the increase in magnitude.

The absolute values of source spectra for the smallest earthquakes are then obtained for the two areas. As mentioned earlier, the source spectra of larger events will be obtained from the relative values of source factors of coda amplitudes for the smallest earthquakes. By using the source term $c(\omega)=[2\,S(\omega)\Delta f]^{1/2}$ which was explained in Eq. (3.1) and (3.2), we obtained the source factors of the coda $[S(\omega)]^{1/2}$. These source factors plotted against the frequency are shown in Figs. 6.6a and 6.6b. These plots are obtained by fixing the factor a in Eq. (3.1) to the value 1 which

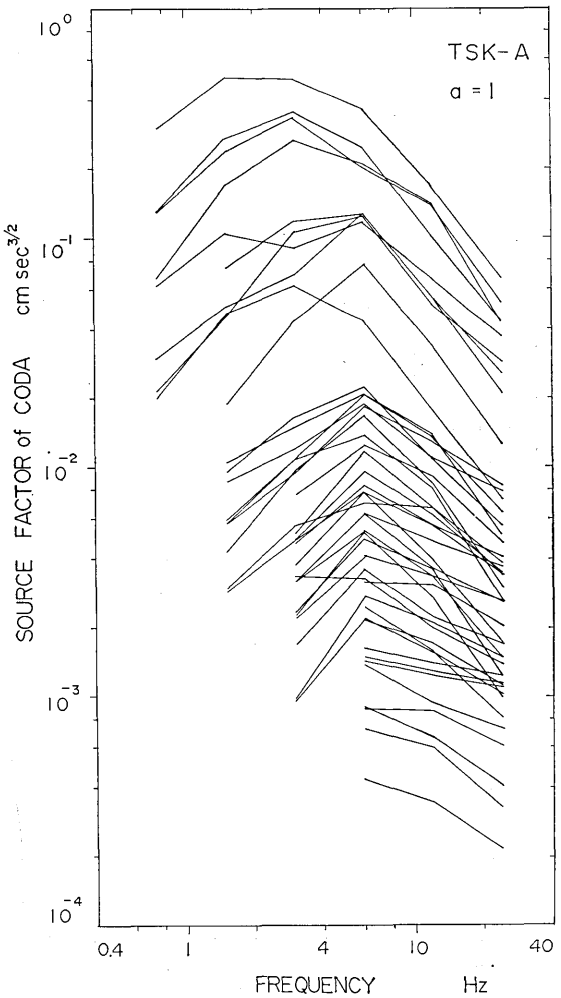

Fig. 6.6a. Source factors of coda waves in the range of 0.75—24 Hz for the events of A area (northern Kanto) recorded at TSK.

is body wave scattering. Each line corresponds to the source factors of an earthquake. The shorter lines define events for which the signals of one or more filter bands are too weak to be measured accurately. The source factors in TSK-A show a somewhat weaker dependence on frequency than in TSK-B, and the dependence of source factors on magnitude is greater at low frequencies and smaller at high frequencies. The growth of the coda source factor may be more clearly seen if we plot the source factor at one frequency as a function of the source factor at another. Figs. 6.7a and 6.7b show the relative growth of the coda spectral amplitude at 12 Hz and 24 Hz versus 3 Hz for the events of TSK-A. Each

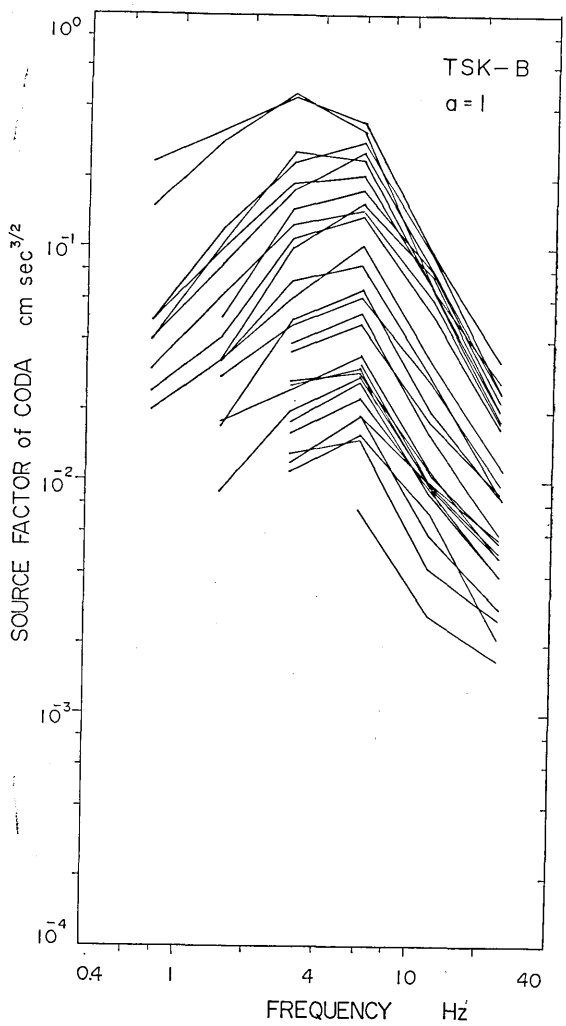

Fig. 6.6b. Source factors of coda waves in the range of 0.75—24 Hz for the events of B area (southern Kanto) recorded at TSK.

point represents an earthquake as derived directly from Fig. 6.6a. The magnitudes of the events used at TSK-A range from 3 to 5.8. The good fit of the straight line indicates the slower rate of increase of the source factors at 12 Hz and 24 Hz as compared to the rate of increase of the source factors at 3 Hz. For example, the average $M=3$ earthquake has a source factor of the coda of 1×10^{-3} cm sec$^{3/2}$ at 3 Hz, and the average $M=5$ event has a source factor of 1.2×10^{-1} cm sec$^{3/2}$ at the same frequency. This relative growth by a factor of 120 in the spectral amplitude at 3 Hz, may be contrasted to the growth at 24 Hz by a factor of 22 for the same magnitude range from 1×10^{-3} cm sec$^{3/2}$ to 2.2×10^{-2} cm sec$^{3/2}$. A similar behavior is seen for the events of TSK-B, and in the events of the California, Hawaii and Tadjikistan regions (CHOUET *et al.*, 1977; RAUTIAN and KHALTURIN, 1976). From Figs. 6.7a and 6.7b, and by making the same measurement at other available filter frequencies, the relative values of the source spectrum for two different earthquakes can be determined from the ratio of the source factors of the coda. In order to fix the absolute values of the source factors we shall use the source spectrum of an M 3.5 earthquake which is already determined (Fig. 6.5a). The source spectra of larger events are thus obtained by using the source factor of coda amplitude relative to that of the reference earthquake.

Fig. 6.8 shows the growth of seismic source spectrum with magnitude, starting with magnitude 1.5 for the two areas. Following the Brune's model (BRUNE, 1970, 1971), the source parameters of seismic moment (M_0), source dimension (r) and stress drop ($\Delta\sigma$) are defined as follows;

$$M_0=4\pi\rho\beta^3\Omega_0 R/KR_{\theta\phi} \tag{6.6}$$

$$r=2.34\beta/2\pi f_c \tag{6.7}$$

$$\Delta\sigma=7/16\ M_0/r^3 \tag{6.8}$$

where Ω_0 is the flat low-frequency spectral level, R is the hypocentral distance, ρ is density, β is the shear-wave velocity, $R_{\theta\phi}$ is the RMS average of the radiation pattern, K is a correction factor for amplification upon free-surface reflection and f_c is the corner frequency. The seismic moment corresponding to each spectral curve was estimated assuming $\beta=4.2$ km/sec, $\rho=2.9$ g/cm^3, $KR_{\theta\phi}=0.85$ (THATCHER and HANKS, 1973), an average hypocentral distance $R=58$ km for TSK-A and 65 km for TSK-B. The value of moment is indicated in the left hand ordinate of Fig. 6.8.

MADARIAGA (1976) calculated the far-field seismic spectrum for circular cracks, and proposed that a radius a of circular crack model can be written as

$$a=0.21\ \beta/f_c \tag{6.9}$$

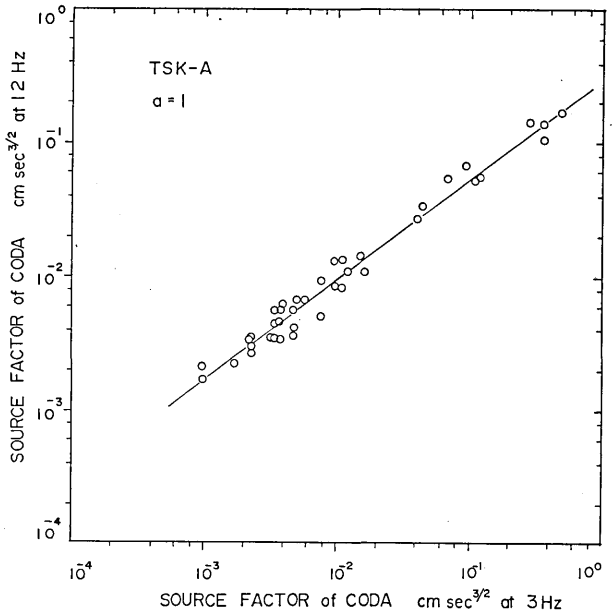

Fig. 6.7a. Relation between coda source factors at 12 Hz and 3 Hz for the events of TSK-A.

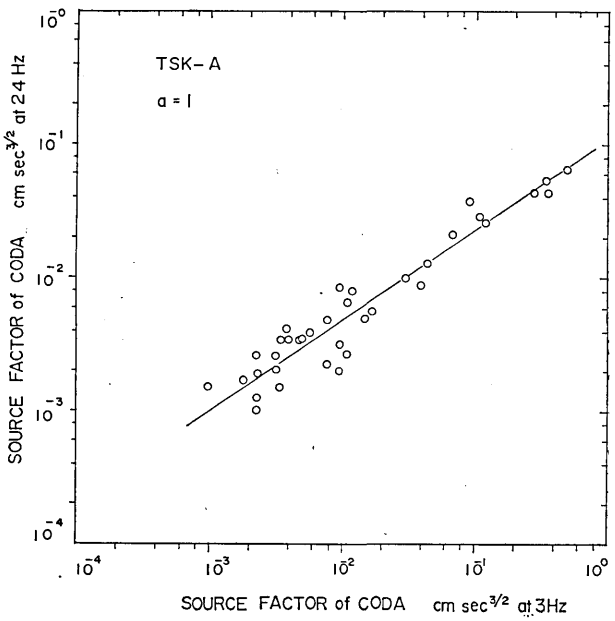

Fig. 6.7b. Relation between coda source factors at 24 Hz and 3 Hz for the events of TSK-A.

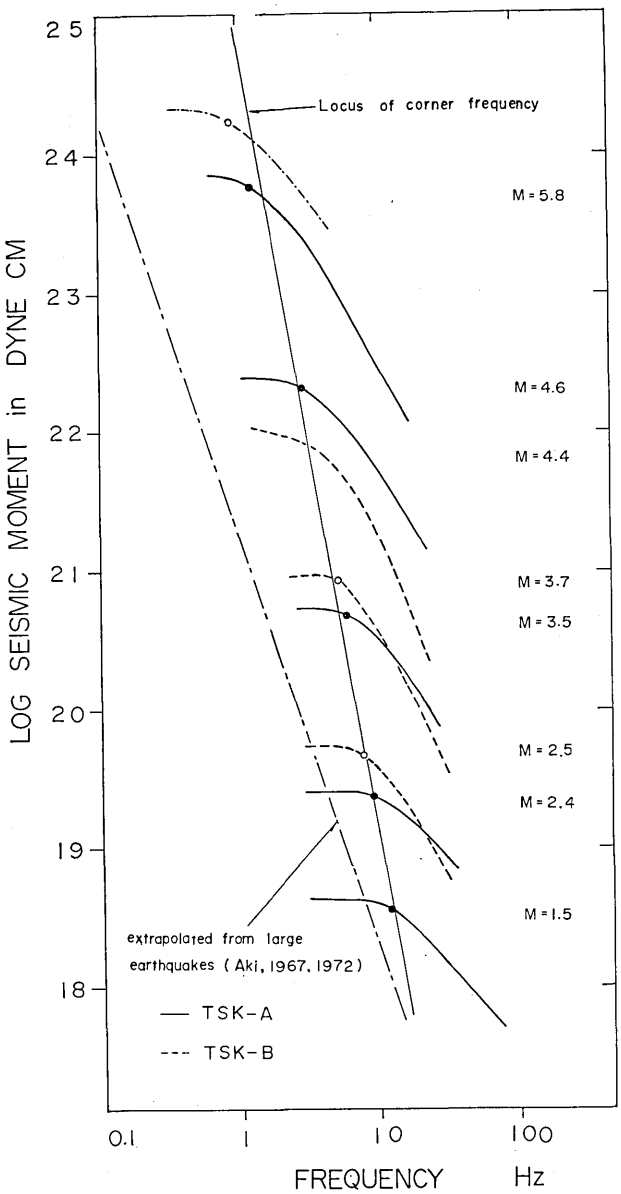

Fig. 6.8. The growth of the seismic source spectra for magnitude from 1.5 to 5.8. Closed and dashed curves indicate the source spectra for the TSK-A and -B, respectively. Dashed-dotted curve indicates the source spectrum of the M 5.8 event obtained from the S wave at DDR. The seismic moment corresponding to each spectral curve is indicated in the left hand ordinate. The locus of the corner frequency appears with the slope of -5 expected the slower rate increasing of the source dimension.

where f_c is the corner frequency for the S wave spectrum and β is the shear wave velocity. Note that the stress drop obtained from formula (6.8) using (6.9) will be about six times larger than that using the Brune's formula.

The scale effect on the spectral shape observed at TSK, when superposed upon the absolute values for $M=1.5$ and $M=3.5$ earthquakes, showed a slow rate of decrease of corner frequency with increasing magnitude from 12 Hz for $M=1.5$ down to 1.2 Hz at $M=5.8$. The apparent good fit of the locus of corner frequency follows a straight line with the steep slope of -5 indicating a very slow rate of increase in the source dimension. Assuming $\beta=4.2$ km/sec by Eq. (6.9) the corner frequencies at 12 Hz and 1.2 Hz correspond to a fault radius of roughly 70 m and 700 m, respectively. The extrapolation of the locus of corner frequency obtained from large earthquakes by AKI (1967, 1972) is shown as a reference. The corner frequency of an $M=5.8$ earthquake is about 10 times greater than Aki's result.

The average $M=1.5$ event with a moment of 4.5×10^{18} dyne cm has a stress drop of about 1 bar, whereas the $M=5.8$ event with a moment of 7.5×10^{23} dyne cm has a stress drop of 150 bars. The stress drop obtained here is estimated by Brune's formula in order to compare the stress drops of the events in the other seismic areas. The stress drop of the $M=5.8$ event is comparable to those obtained for the larger aftershocks ($M_0>10^{21}$ dyne cm) of the San Fernando earthquake (TUCKER and BRUNE, 1973) and the smaller value is also comparable to those obtained by WYSS (1970), DOUGLAS and RYALL (1972), TUCKER and BRUNE (1973), ISHIDA, (1974), and BAKUN and BUFE (1975). On the other hand, THATCHER (1972), and THATCHER and HANKS (1973) suggested that the stress drops vary from tenths of a bar to 200 bars, and there is no significant trend as a function of magnitude. However, as shown in Eq. (6.8), the stress drop depends on $1/r^3$, it is therefore very sensitive to a small error in the source dimension determined by the corner frequency. Moreover, our spectrum analyzer is taken from the output of a 1 Hz seismometer. Spectral amplitudes of less than about 1.5 Hz are made somewhat uncertain by the characteristics of a seismograph where the magnification is lower than 1/10 for the peak magnification. In order to check the facts described above, the source parameter of the $M5.8$ earthquake is examined by using the data of DDR where various seismographs are operating (TSUJIURA, 1965, 1973b). Fig. 6.9 shows the original seismograms recorded on long-period (LP) and ultra long-period (ULP) seismographs. High frequency S waves with about 1 Hz are clearly demonstrated on the ULP seismogram which has a flat response between 1 Hz and 0.01 Hz. The spectral analysis for SH waves (N-S) is made by the analog-filtering method (TSUJIURA,

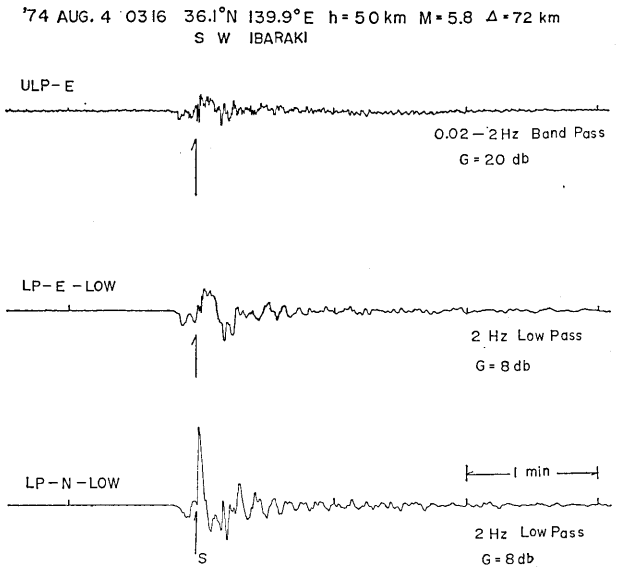

Fig. 6.9. Original seismograms for the M5.8 earthquake recorded on long-period (LP) and ultra long-period (ULP) seismographs at DDR.

1973b). As shown in section 5, DDR has a different site effect than TSK (Fig. 5.3), the amplitudes of frequencies lower than 3 Hz therefore are divided by factors of 3 for $f \leq 1.5$ Hz and 2 for $f = 3$ Hz. Correcting by a value of Q_β 600 which was obtained by the same method at TSK (Eq. 6.5) and the site factor, the source spectrum determined for SH waves is shown by a dash-dotted curve in the same figure. Using Brune's formula the values of M_0 and $\Delta\sigma$ are obtained as 2×10^{24} dyne cm and 200 bars, respectively.

Another check of our result is the comparison with the source parameter of the M6.1 earthquake that occurred at the TSK-A. ABE (1975) made a detailed analysis on the basis of the data on P-wave first motions, aftershock distribution, teleseismic surface waves and long-period seismograms recorded in the near-field to determine the source parameter of this earthquake, and obtained the values of the moment of 1.9×10^{25} dyne cm and a stress drop of 100 bars. Our finding for the M5.8 earthquake gives a reasonable value in the light of Abe's results if we consider the variation of source spectra for an individual earthquake and the sensitivity of the estimation of corner frequency. Thus, it will be concluded that the high stress drop of the M5.8 event is not caused by instrumental error. On the other hand, long-period data will be needed for larger events of the TSK-B area as discuss later. TSUJIURA (1969), WYSS (1970), and WYSS and BRUNE (1971) showed that the spectrum of body waves

varies as a function of depth. The greater stress drop therefore may be due to the deeper source ($h=50$ km) where greater effective stress will be expected. The small stress drop for smaller events is also understandable if we assume that the rupture strength of the rock varies from place to place in the crust, and small events occur in places with relatively weak rupture strength.

The high frequency asymptote is slightly different for areas A and B. Although the corner frequency of $M3.5$ events is the same, the 30 Hz spectral density for the earthquake at the TSK-A is 4 times as large as that of the TSK-B as the result of the different scaling law of source spectra. The difference of the source spectra between the two areas becomes more clear for larger events. The 15 events with magnitudes of 4.3–5.0 and source depths of 50 km–70 km have recently been obtained on magnetic tape at DDR. The event parameters of these events given by the Japan Meteorological Agency (JMA) is listed in Table 6. Fig. 6.10 shows a typical example of seismograms recorded by the long-period (LP) and wide-band (WB) seismographs for two events that occurred in the areas A and B. In spite of the fact that they have almost the same magnitude (M), source depth (h) and epicentral distance (Δ), clear differences in amplitude and period can be seen on both LP and WB seismograms.

Table 6. List of event and source parameters.
h: source depth in km, M: magnitude, f_c: corner frequency in hertz, a: source radius in km. *: magnitude is determined by the total duration time of seismogram at DDR.

Date	Time h m s	Epicenter degree		h km	M	f_c Hz	a km
73 Dec. 22	10 19 59.7	35°13′ N	140°17′ E	70	4.7*	0.8	1.1
74 May 30	16 12 04.1	36 31 01 N	140 37 02 E	60	4.3*	2.2	0.45
74 Sep. 29	01 01 08.5	36 28 01 N	140 36 02 E	60	4.3	2.5	0.35
74 Oct. 09	04 09 16.6	36 00 01 N	139 57 01 E	50	4.6	1.8	0.49
74 Oct. 09	04 42 08.5	36 03 01 N	139 55 01 E	60	4.8	1.5	0.59
74 Oct. 29	20 00 00.3	35 36 01 N	140 20 01 E	70	4.9	0.3	2.9
74 Oct. 30	00 56 57.7	35 36 01 N	140 21 02 E	60	4.5	0.32	2.8
74 Nov. 01	18 41 56.9	35 36 01 N	140 20 01 E	60	4.3	0.36	2.5
74 Nov. 21	20 59 29.3	35 37 01 N	140 20 02 E	60	4.7	0.28	3.2
75 Apr. 12	07 15 48.3	36 06 01 N	140 01 01 E	50	5.0	1.8	0.49
75 Apr. 18	03 41 08.4	36 08 01 N	139 51 01 E	50	5.0	1.4	0.63
75 Apr. 21	12 45 15.2	36 30 01 N	140 42 02 E	60	4.8	1.2	0.73
76 June 06	23 01 21.2	36 03 01 N	139 40 01 E	70	4.8	1.3	0.68
76 July 18	04 57 24.9	36 27 01 N	140 36 01 E	50	4.4*	2.4	0.37
76 Aug. 04	08 37 45.4	36 11 01 N	139 50 01 E	60	4.7	1.2	0.73

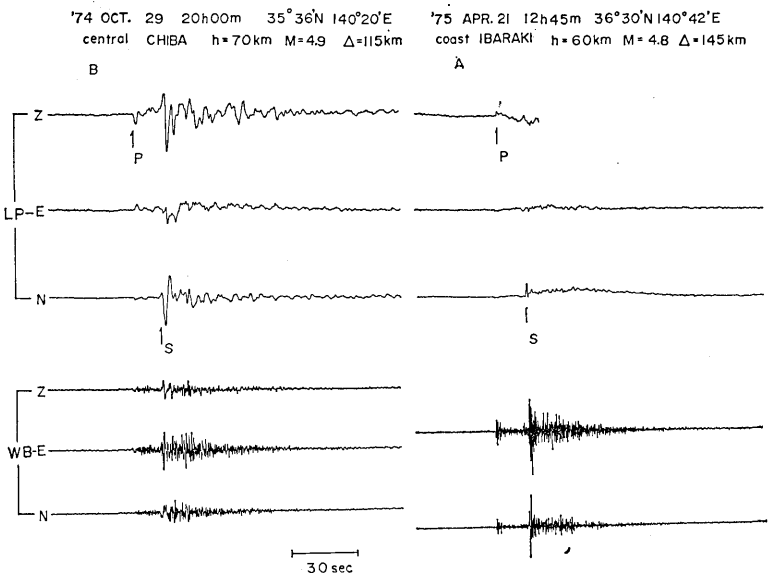

Fig. 6.10. A comparison of seismograms of two earthquakes with almost the same magnitude (M), source depth (h) and distance (Δ) recorded on long-period (LP) and wide-band (WB) seismographs at DDR. Note the clear difference in the low- and high frequency amplitudes of waves from the typical northern Kanto event (A), contrasting with the waveforms of the event for southern Kanto (B).

Relatively short-period S waves (0.75 sec) are predominant on the LP and WB seismograms for the event A, in contrast to longer period (4 sec) for the event B. After the correction of amplitudes by the response curves of LP and WB, both events give similar ground displacement within a factor of 1.5. Although we have no detailed knowledge of the propagation path effect for either event, the difference of waveforms will be predominantly the result of contrasting source properties.

A rough estimation of Q_β by using the Eq. (6.5) gives a value of 600 and 350 for the areas of DDR-A and DDR-B, respectively. If we use these values for correction, there is no marked difference on the amplitudes of frequencies lower than 2 Hz when the hypocentral distance is less than 100 km. Using the same method described above, the source spectrum of each event is obtained. The source radii obtained from the SH wave assuming $\beta=4.2$ km/sec by Eq. (6.9) are listed in Table 6 together with the corner frequencies estimated. The relative difference of source sizes is also shown schematically in Fig. 6.11 for an easy comparison. Numerals attached to the circles represent their magnitude. The difference of source dimensions becomes more than a factor of 8 even in the same magnitude and average 4.7. The low frequency level of the source

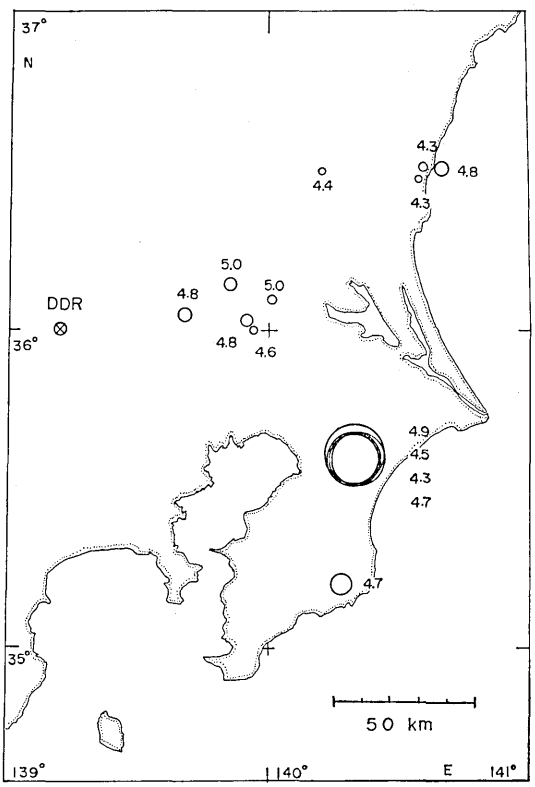

Fig. 6.11. Map showing schematically the local differences of source size derived from the corner frequency for the events with magnitudes of 4.3 to 5.0 and whose depths range from 50 to 70 km. Numerals attached to the circles show their magnitudes.

spectra of these events is almost the same, within a factor of two when the events with the same magnitude are compared. Therefore the difference of the stress drop determined from the Eqs. 6.6 and 6.8 is roughly from 50 to 100 times. Although the epicenters of earthquakes presented here are located in a limited area, the source spectra for larger events, $M \geq 4.3$, may be changed systematically between the areas A and B. Different stress drops for different shocks of the same magnitude probably result from their different tectonic environment. It seems reasonable to expect that a low stress drop and large source dimensions will be associated with earthquakes occurring in zones of weakness as suggested by WYSS and BRUNE (1971). After the collection of much more data with different locations, and correlating the stress drop and fault radii, we shall construct the final scaling law to predict the strong motions of great earthquakes in the Kanto district.

The scaling law of the seismic spectra proposed by AKI (1967) was

based on a similarity assumption for large and small earthquakes. This assumption implies a constant stress drop in all earthquakes. However, the result of the present study demonstrated that the stress drop may depend on the earthquake magnitude or the seismic area. Local variation of the source spectra must be taken into account in assessing their scaling law. This fact has an important implication in predicting seismic spectra of great earthquakes. It will be useful for earthquake engineering and seismic zoning.

7. Conclusion

The spectral content and decay characteristics with time of coda waves from local earthquakes are studied using the data of six stations distributed in the Kanto district, and some properties of attenuation, excitation and source effects of the coda waves are obtained.

The decay characteristics of coda waves determined at a given station are independent of the epicenter location and source size, and it depends only upon the duration time measured from the origin time as suggested by AKI (1969). The apparent Q of coda waves obtained from four stations increases with frequency, approximately proportionally to the square root of their frequency, with values increasing from 120–250 at 0.75 Hz to 800–2500 at 24 Hz. Close scrutiny of these values shows that there is a local feature, which depends on the local geology of station site. For example, the increasing of Q with frequency is less pronounced in KYS, located on the sandstone layer, showing values of 250 at 0.75 Hz and 800 at 24 Hz. On the other hand, the increase of Q at TSK, located on the granitic rocks, is large, especially for deeper events, showing values of 150 at 0.75 Hz and 2500 at 24 Hz.

The coda amplitude observed at different stations depends on frequency, and it also correlates with the local geology of the station site. The differences of coda amplitudes between the stations located on sediment and granitic rocks are, on the average 20 times at 0.75 Hz and less than 1/10 at 24 Hz. This may be attributed to the differences in intrinsic Q and inhomogeneity size of the earth's crust beneath the station. These tendencies are the same for those of S waves. The station correction for the site factor as well as the correction for attenuation must be applied to the spectra for the determination of source spectra. The spectral comparison of coda waves from local earthquakes may be used to obtain the site factors for a wide frequency band.

The scaling law of earthquake source spectra is constructed by use of the spectral ratios of coda source factors and the source spectra of the smallest earthquakes used in the estimation of coda source factors. A

marked difference in the scaling law for the source spectra is found within the area of the Kanto district, which may be attributed to the difference in rupture strength of the earth's crust. The seismic moments of earthquakes in northern Kanto with magnitudes from 1.5 to 5.8 are from 4.5×10^{18} to 7.5×10^{23} dyne cm. The locus of corner frequency for the source spectra of these earthquakes shows a straight line with f^{-5} from 12 Hz for $M=1.5$ down to 1.2 Hz for $M=5.8$. On the other hand, the corner frequency of large events ($M\geq4.3$) in southern Kanto is quite small, on the average 0.3 Hz for $M=5$ events although the corner frequencies of smaller events ($M<3.5$) have the same value. The values of stress drop for $M=5$ events in northern and southern Kanto are about 100 bars and 1 bar, respectively.

Acknowledgment

The writer wishes to express his thanks to Prof. Keiiti Aki who read the manuscript critically and offered many valuable suggestions. The writer also thanks Drs. Megumi Mizoue and Katsuyuki Abe for their valuable advice, and Dr. Kenshiro Tsumura for the use of unpublished data of epicenter determination. Gratitude is expressed to the National Research Center for Disaster Prevention for the use of the seismic signals of Iwatsuki station.

References

ABE, K., 1975, Static and dynamic fault parameters of the Saitama earthquake of July 1, 1968, *Tectonophysics*, **27**, 223-238.

AKI, K., 1967, Scaling law of seismic spectrum, *J. Geophys. Res.*, **72**, 1217-1231.

AKI, K., 1969, Analysis of the seismic coda of local earthquakes as scattered waves, *J. Geophys. Res.*, **74**, 615-631.

AKI, K., 1972, Scaling law of earthquake source time-function, *Geophys. J. R. Astr.* Soc., **31**, 3-25.

AKI, K., 1973, Scattering of *P* waves under the Montana Lasa, *J. Geophys. Res.*, **78**, 1334-1346.

AKI, K. and B. CHOUET, 1975, Origin of coda waves: source, attenuation, and scattering effects, *J. Geophys. Res.*, **80**, 3322-3342.

BAKUN W. H. and C. G. BUFE, 1975, Shear-wave attenuation along the San Andreas fault zone in central California, *Bull. Seism. Soc. Am.*, **65**, 439-459.

BARAZANGI, M. and B. ISACKS, 1971, Lateral variations of seismic-wave attenuation in the upper mantle above the inclined earthquake zone of Tonga Island arc: deep anomaly in the upper mantle, *J. Geophys. Res.*, **76**, 8493-8516.

BRUNE, J. N., 1970, Tectonic stress and the spectra of seismic shear waves from earthquakes, *J. Geophys. Res.*, **75**, 4997-5009.

BRUNE, J. N., 1971, Correction, *J. Geophys. Res.*, **76**, 5002.

CAPON, J., 1974, Characterization of crust and upper mantle structure under Lasa as a random medium, *Bull. Seism. Soc. Am.*, **64**, 235-266.

CHOUET, B. A., 1976, Source, scattering and attenuation effects on high frequency seismic waves, *Ph. D. Thesis*, Massachusetts Institute Technology.

CHOUET, B., K. AKI and M. TSUJIURA, 1977, Regional variation of the scaling law of earthquake source spectra, *Bull. Seism. Soc. Am.*, in press.

CLEARY, J. R. and R. A. W. HADDON, 1972, Seismic wave scattering near the core-mantle boundary: A new interpretation of precursors to *PKIKP*, *Nature*, **240**, 549-550.

DOUGLAS, B. M. and A. RYALL, 1972, Spectral characteristics and stress drop for micro-earthquake near Fairview peak, Nevada, *J. Geophys. Res.*, **77**, 351-359.

FEDOTOV, S. A., A. A. GUSEV and S. A. BOLDYREV, 1972, Progress of earthquake prediction in Kamchatka, *Tectonophysics*, **14**(3/4), 279-286.

ISHIDA, M., 1974, Determination of fault parameters of small earthquakes in the Kii peninsula, *J. Phys. Earth*, **22**, 177-212.

JOHNSON L. R. and T. V. MCEVILLY, 1974, Near-field observations and source parameters of central California earthquakes, *Bull. Seism. Soc. Am.*, **64**, 1855-1886.

MADARIAGA, R., 1976, The dynamics of an expanding circular fault, *Bull. Seism. Soc. Am.*, **66**, 639-666.

MIYAMURA, S. and S. YAMADA, 1973, Detection capability of *P* arrival times at the station DDR, TSK and KYS belonging to the Dodaira Micro-earthquake Observatory, *Spect. Bull. Earthq. Res. Inst.*, **10** (4), 5-24, (in Japanese).

OMOTE, S., 1943, On the coda waves of the earthquake motions (part 1), *Bull. Earthq. Res. Inst.*, **21**, 458-500, (in Japanese).

PEKERIES, C. L. and H. LIFSON, 1957, Motion of the surface of a uniform elastic half-space produced by a buried pulse, *J. Acoust. Soc. Amer.*, **29**, 1233-1238.

RAUTIAN T. G. and V. I. KHALTURIN, 1976, The frequency-temporal properties of coda waves for local earthquakes of Garm region, USSR, (preprint).

SHIMA, E. *et al.*, 1976, On the base rock of Tokyo. Observations of seismic waves generated from the 1st and 2nd Yumenoshima explosions, *Bull. Earthq. Res. Inst.*, **51**, 1-11, (in Japanese).

TAKAHASHI, H. and K. HAMADA, 1975, Deep borehole observation of the earth's crust activities around Tokyo—Introduction of the Iwatsuki observatory, *Pure and applied Geophysics*, **113**, 311-320.

TAKAHASI, R. and K. HIRANO, 1941, Seismic vibrations of soft ground, *Bull. Earthq. Res. Inst.*, **19**, 534-543, (in Japanese).

TAKANO, K., 1971, Analysis of seismic coda waves of ultra microearthquakes in the Matsushiro area -A comparison with Parkfield, California, *J. Phys. Earth*, **19**, 209-216.

TANAKA, T., S. YOSHIZAWA, T. MORISHITA, K. OSADA and Y. ŌSAWA, 1973, Observation and analysis of underground earthquake motions, *Proc. 5 WCEE*, **1**, 658-667.

THATCHER, W., 1972, Regional variations of seismic source parameters in the northern Baja California area, *J. Geophys. Res.*, **77**, 1549-1565.

THATCHER, W. and T. C. HANKS, 1973, Source parameters of southern California earthquakes, *J. Geophys. Res.*, **78**, 8547-8576.

TSUJIURA, M., 1965, A pen-writing long-period seismograph, part 3, *Bull. Earthq. Res. Inst.*, **43**, 429-440, (in Japanese).

TSUJIURA, M., 1966, Frequency analysis of seismic waves (1), *Bull. Earthq. Res. Inst.*, **44**, 873-891.

TSUJIURA, M., 1967, Frequency analysis of seismic waves (2), *Bull. Earthq. Res. Inst.*, **45**, 973-995.

TSUJIURA, M., 1969, Regional variation of *P* wave spectrum (1), *Bull. Earthq. Res. Inst.*, **47**, 613-633.

TSUJIURA, M., 1972, Spectra of body waves and their dependence on source depth 1. Japanese arc, *J. Phys. Earth*, **20**, 251-266.

TSUJIURA, M., 1973a, Regional variation of micro-earthquake spectrum—Kanto district,—

Zisin, **26**, 370-375, (in Japanese).

TSUJIURA, M., 1973b, Spectrum of seismic waves and its dependence on magnitude (1), *J. Phys. Earth*, **21**, 373-391.

TSUJIURA, M., 1977, Spectral features of foreshocks, *Bull. Earthq. Res. Inst.*, **52**, 357-371.

TSUMURA, K., 1973, Microearthquake activity in the Kanto district, Pub., 50th Anniversary of the great Kanto earthquake, 1923, *Earthq. Res. Inst.*, 67-87, (in Japanese).

TUCKER, B. E. and J. N. BRUNE, 1973, Seismogram, *S*-wave spectra and source parameters for aftershocks of the San Fernando earthquake of February 9, 1971, in geological and geophysical studies, vol. 3, San Fernando earthquake of February 9, 1971, *National Oceanic and Atomospheric Administration, Washington, D. C.*

WYSS, M. and J. N. BRUNE, 1968, Seismic moment, stress and source dimensions for earthquakes in the California-Nevada region, *J. Geophys. Res.*, **73**, 4681-4694.

WYSS, M., 1970, Stress estimates for south American shallow and deep earthquakes, *J. Geophys. Res.*, **75**, 1529-1544.

WYSS, M. and J. N. BRUNE, 1971, Regional variations of source properties in southern California estimated from the ratio of short-to long-period amplitudes, *Bull. Seism. Soc. Am.*, **61**, 1153-1167.

1. 近地地震 Coda Wave のスペクトル解析

地震研究所　辻　浦　　賢

関東地方に分布する観測所6ヶ所のデーターを用い，近地地震 Coda Wave について調べ，その性質についていくつかの結果を得た．解析は約 1 Hz から 30 Hz について6チヤンネルに分割したバンドパスフイルターの記録により行なった．

1) ある観測所で得られる Coda Wave の減衰特性はそれ等の地震の震源位置，伝播経路及び大きさに略無関係であって，その減衰は夫々の地震の発震時から測った経過時間のみに依存する．周波数別の振巾の減衰特性から求めた Q の値は，周波数に依存し，0.75 Hz で 150−250, 24 Hz で 800−2500 の値を得た．更に詳しくみるとこれらの値は観測点の地盤構造に依存し，例えば砂岩層に位置する清澄 (KYS) では，低周波領域で比較的大きく (250, 1 Hz)，高周波領域で逆に小さい (800, 24 Hz)．一方花崗岩層に位置する筑波 (TSK) では逆の傾向を示し，特に深発地震 ($h>100$ km) から求めた高周波での Q は 2500 にも達する．

2) Coda Wave の振巾は観測点の地盤特性に依存し，発震時から測った同じ経過時間での振巾の違いは最大 20 倍にも達する．例えばたい積層に位置する地震研究所地下地震計室では筑波に比較し，0.75 Hz で約 20 倍大きく，逆に 24 Hz で 1/10 以下である．

3) Coda Wave のスペクトル比と取り扱った最小地震の震源スペクトルから，地震の大きさと震源スペクトルの関係を求めた．関東地方の地域内でこれらの値は一様ではなく，特に大きい地震 ($M\geq 4.3$) でその違いは顕著である．例えば Source dimension についてみると，南関東では北関東にくらべ $M\approx 5$ の地震で約 4 倍大きい．

今後地震計の帯域巾を広げ，低周波領域における Coda Wave の振巾と地盤特性の関係，更に資料の蓄積をまって，地震の大きさと震源スペクトルの関係を求め，同地域における大地震の震源スペクトルを推定することを目的にこの種の観測を続けてゆきたい．